Macrophage SLC9A1 Links Endocytic Trafficking to Innate Immune Activation in Myocardial Injury

Jinhua Wen[1*], Pablo Parra[1*], Yoshi Muto[2], Guo Chen[1], MariaSanta C Mangione[3], Xiang Luo[1], Dian J Cao[1,4]

[1]Department of Internal Medicine
Cardiology Division
University of Texas Southwestern Medical Center
Dallas, TX 75390
USA

[2]Department of Internal Medicine
Nephrology Division
University of Texas Southwestern Medical Center
Dallas, TX 75390
USA

[3]Department of Internal Medicine
University of Texas Southwestern Medical Center
Dallas, TX 75390
USA

[4]Department of Internal Medicine
Cardiology Division
Dallas VA Medical Center
1400 S. Lancaster Road
Dallas, TX
USA

Running Title: SLC9A1 regulates macrophage function in MI

* Authors contributed equally

To whom correspondence should be addressed:

Dian Cao, MD, PhD
Division of Cardiology,
UT Southwestern Medical Center
6000 Harry Hines Blvd
Dallas, TX 75390-8573
Tel: 1-214-648-1400
Fax: 1-214-648-1450
Twitter: @DrDianCao
Dian.Cao@utsouthwestern.edu

Abstract

Excessive innate immune activation contributes to adverse remodeling following myocardial infarction (MI), yet the upstream mechanisms governing macrophage sensing of ischemic danger signals remain incompletely defined. Here, we investigated whether macropinocytosis functions as a critical checkpoint for post-ischemic inflammation and whether the Na^+/H^+ exchanger SLC9A1 regulates this process in monocytes and macrophages. We hypothesized that macropinocytosis-dependent uptake of damage-associated molecular patterns amplifies inflammatory signaling after MI and that SLC9A1 selectively enables delivery of nucleic acid ligands to endosomal pattern-recognition receptors.

We demonstrate that macropinocytosis is robustly activated in infarct-associated macrophages, which represent the predominant macropinocytic population in the injured heart. Pharmacologic inhibition of macropinocytosis with 5-(N-ethyl-N-isopropyl)amiloride (EIPA) improved cardiac function and attenuated post-MI remodeling. To define macrophage-intrinsic mechanisms, we generated monocyte- and monocyte-derived macrophage–specific Slc9a1 knockout mice. Genetic deletion of Slc9a1 phenocopied the cardioprotective effects of EIPA and markedly suppressed interferon-stimulated gene expression in infarct-associated macrophages, as revealed by single-cell RNA sequencing. Mechanistically, SLC9A1 facilitated poly(I:C) endocytosis and enhanced TLR3-dependent signaling, linking macropinocytosis to endosomal innate immune activation. Notably, EIPA also suppressed cardiac inflammatory responses induced by systemic poly(I:C) and lipopolysaccharide, extending these findings to models of viral and bacterial challenge.

Together, our data identify macrophage macropinocytosis as a central regulator of innate immune activation after MI and establish SLC9A1 as a key modulator of endosome-dependent TLR signaling. These findings uncover a previously unrecognized link between membrane dynamics and inflammatory injury and suggest that targeting SLC9A1-dependent pathways may offer therapeutic potential in myocardial ischemia and systemic inflammatory diseases.

Introduction

Acute myocardial infarction (MI) triggers a robust inflammatory response that is essential for debris clearance but, when excessive or prolonged, drives adverse cardiac remodeling and progression to heart failure. Innate immune activation is a central component of this response, with macrophages serving as key orchestrators of post-ischemic inflammation, tissue repair, and remodeling. Multiple pattern recognition receptors (PRRs), including Toll-like receptor 3 (TLR3) and Toll-like receptor 4 (TLR4), are activated in the infarcted myocardium, reflecting exposure to damage-associated molecular patterns (DAMPs) and endogenous nucleic acids released from necrotic cardiomyocytes[1, 2]. However, despite extensive characterization of PRR signaling pathways, a critical mechanistic question remains unresolved: how extracellular danger signals gain intracellular access to engage endosomal innate immune sensors in post-infarction macrophages.

Macropinocytosis is a high-capacity, actin-dependent endocytic pathway through which cells internalize large volumes of extracellular fluid and soluble cargo, including proteins and nucleic acids[3-6]. Unlike receptor-mediated endocytosis, macropinocytosis is strongly induced by cellular stress, growth factor signaling, and tissue injury, conditions that are prominent within the ischemic myocardium. In myeloid cells, bulk and endocytic uptake pathways, including macropinocytosis can promote delivery of extracellular nucleic-acid cargo to endolysosomal compartments, enabling activation of intracellular PRRs and downstream inflammatory[7]. Despite these properties, the role of macrophage macropinocytosis in myocardial ischemia has not been examined, and whether this uptake pathway contributes to inflammatory amplification following MI remains unknown.

Macrophages are highly plastic cells that continuously survey their microenvironment and dynamically adjust their functional states in response to local cues[8, 9]. To support this surveillance, macrophages internalize membrane equivalent to their entire cell surface approximately every 30–35 minutes[10], with macropinocytosis accounting for a substantial fraction of this uptake. Following MI, the necrotic myocardium releases abundant DAMPs, including nucleic acids and proteins, that are well suited for internalization via macropinocytosis. Once internalized, these danger signals may engage endosomal PRRs to initiate inflammatory signaling, while simultaneously providing metabolic substrates that support macrophage survival and mTORC1 activation[11] in nutrient-restricted ischemic tissue. Through these dual functions, macropinocytosis is positioned to coordinate inflammatory sensing and metabolic adaptation in infarct-associated macrophages.

Solute carrier family 9 member A1 (SLC9A1), also known as the Na^+/H^+ exchanger 1 (NHE1), is a ubiquitously expressed plasma membrane antiporter that plays a fundamental role in intracellular pH and

volume homeostasis. By extruding intracellular protons in exchange for extracellular sodium ions, SLC9A1 counteracts cytosolic acidification and facilitates osmotic swelling required for membrane expansion[12]. Beyond its canonical role in pH regulation, SLC9A1 regulates actin cytoskeletal organization, membrane ruffling, and endosomal dynamics[13, 14], processes that are integral to macropinocytosis. Pharmacological inhibition of Na^+/H^+ exchangers has been shown to suppress macropinocytic uptake in macrophages, implicating SLC9A1 as a potential regulator of macropinocytosis-dependent immune sensing.

Despite extensive study of SLC9A1 in excitable tissues such as the heart and brain, its function in monocytes and macrophages remains poorly defined. Emerging evidence links SLC9A1 to macrophage-driven foam cell formation and atherogenesis, yet studies of SLC9A1 in acute cardiovascular inflammation have largely focused on cardiomyocytes, leaving its role in macrophages unexplored. This gap is notable given that SLC9A1 is the predominant Na^+/H^+ exchanger isoform expressed in macrophages[15, 16] and that therapeutic inhibition of this transporter has been proposed in atherosclerosis[17, 18]. Whether SLC9A1 regulates macrophage inflammatory responses during MI by controlling macropinocytosis and danger signal sensing has not been determined.

In this study, we investigated whether macropinocytosis functions as a critical checkpoint for innate immune activation following myocardial ischemia and whether SLC9A1 contributes to this process in monocytes and macrophages. We hypothesized that macropinocytosis-dependent uptake of danger signals amplifies post-MI inflammation and that SLC9A1 selectively enables this process by facilitating delivery of nucleic acid ligands to endosomal PRRs. To test this hypothesis, we first assessed whether macropinocytic activity is engaged in macrophages within the infarcted myocardium and whether pharmacologic inhibition of this pathway confers protection from ischemic injury.

To define the macrophage-intrinsic role of SLC9A1, we generated monocyte- and monocyte-derived macrophage (MDM)–specific deletion of Slc9a1 and performed single-cell RNA sequencing (scRNA-seq) on infarct-associated MDMs. In parallel, we employed siRNA-mediated knockdown approaches and selective PRR ligands, poly(I:C) for TLR3 and lipopolysaccharide (LPS) for TLR4, to delineate the mechanistic relationship between SLC9A1, macropinocytosis, and innate immune signaling. To assess translational relevance, we further examined the effects of pharmacologic macropinocytosis inhibition using 5-(N-ethyl-N-isopropyl)amiloride (EIPA), an amiloride analog widely used experimentally and clinically, and evaluated the extent to which pharmacologic inhibition recapitulates the effects of genetic Slc9a1 deletion. Finally, we extended these analyses to models simulating systemic viral and bacterial

challenge to determine whether macropinocytosis-dependent immune regulation generalizes beyond myocardial injury.

Material and method.

Animals.

Animals were kept in a pathogen-free environment with free access to food and water. They were maintained on a 12-hour light/dark cycle from 6 am to 6 pm. All procedures were approved by the Institutional Animal Care and Use Committee at the University of Texas Southwestern Medical Center. The *Nhe1*$^{flox/flox}$ mice were kindly provided by Dr. Dandan Sun from the University of Pittsburgh. The Ccr2-CreER-GFP mice were from JAX (#:035229). The *Nhe1*$^{flox/flox}$ and the *Ccr2-CreER-GFP* are cross bred to generate the compound mice *Nhe1*$^{flox/flox}$ and the *Ccr2-CreER-GFP.* To induce *Nhe1* deletion from monocytes, tamoxifen was administered via ip injection at 10mg/kg for five days followed by a seven days wash-off period. Control cohorts, *Ccr2-CreER-GFP* and *Nhe1*$^{flox/flox}$ received the same amount and duration of tamoxifen treatment. Baseline echocardiogram was performed before and after tamoxifen injection. All mice are from the C57BL/6J background.

Reagents.

The antibodies and the sources of these antbodies are listed in the following table. Reagents used are described in specific experiments.

P-S6 Rabbit mAb	4858S	MyBiosource
Mouse S6 Ribosomal Protein Monoclonal Antibody	MBS475585	mybiosource
mTOR antibody	MBS9131453	Fitzgerald
GAPDH ANTIBODY	10R-G109A	Cell Signaling Technologies
Phospho-NF-κB p65 (Ser536) (93H1) Rabbit mAb	3033T	Cell Signaling Technologies
NFkB, NF-κB p65 (D14E12) XP® Rabbit mAb	8242T	Fisher Scientific
CD68 antibody | FA-11, Rat anti Mouse CD68	MCA1957GA	Cell Signaling Technologies
p-ERK	9101S	Cell Signaling Technologies
ERK	9107S	Cell Signaling Technologies
Toll-like Receptor 4 (D8L5W) Rabbit mAb	14358S	Cell Signaling Technologies
Phospho-Akt (Ser473) (D9E) XP® Rabbit mAb	4060S	Cell Signaling Technologies
akt 308 (Phospho-Akt (Thr308) (244F9) Rabbit mAb	4056S	Cell Signaling Technologies
Phospho-p70 S6 Kinase (Thr389) Antibody	9205S	Cell Signaling Technologies
Akt (pan) (40D4) Mouse mAb	2920S	Cell Signaling Technologies
S6 Ribosomal Protein (54D2) Mouse	2317S	Cell Signaling Technologies
Tuberin/TSC2 (D93F12) XP® Rabbit mAb	4308T	Cell Signaling Technologies
Phospho-Tuberin/TSC2 (Thr1462) (5B12) Rabbit mAb	3617T	Cell Signaling Technologies
4E-BP1 (53H11) Rabbit mAb	9644S	Cell Signaling Technologies
Phospho-4E-BP1 (Thr37/46) (236B4) Rabbit mAb	2855S	Life technologies

POLR3F Polyclonal Antibody	PA520589	Cell Signaling Technologies
Phospho-PI3 Kinase p85 (Tyr458)/p55 (Tyr199) (E3U1H)	17366	Cell Signaling Technologies
PI3 Kinase p85 Antibody	4292	Cell Signaling Technologies
IL-1β (D6D6T) Rabbit mAb	#31202	Proteintech
NHE1 Polyclonal antibody	29761-1-AP	Novus Biologicals
MyD88 Antibody (316902)	MAB3109-SP	Novus Biologicals
phospho GsK3a/b (Ser21/9)	9327S	Cell Signaling Tech.
GSK-3beta	610202	BD
mTOR	2972	Cell Signaling Technologies
mTOR (L2Td4)	4517s	Cell Signaling Technologies
mTOR (7C10)	2983	Cell Signaling Technologies
phospho mTOR (ser2481)	2974	Cell Signaling Technologies

Mouse myocardial infarction model.

A murine model of myocardial infarction was employed involving permanent ligation of the left anterior descending coronary artery (LAD) as described previously23, 56. Briefly, 10-16 weeks old cGas-/- and Sting-/- mice, their WT littermates, and WT animals of the same genetic background were anesthetized with 2.4% isoflurane and positioned supine on a heating pad (37°C). Tracheal intubation was performed with a 19G stump needle, and animals ventilated with room air using a MiniVent mouse ventilator (Hugo Sachs Elektronik; stroke volume, 250 μL; respiratory rate, 210 breaths per minute). Following left thoracotomy between the fourth and fifth ribs, the LAD was visualized under a microscope and ligated with 6-0 Prolene suture. The suture was placed at the LAD segment corresponding to 1.5 mm to 2 mm below the lower edge of the left atrium. Regional ischemia was confirmed by visual inspection of discoloration of myocardium distal to the occlusion under a dissecting microscope (Leica). Sham-operated animals underwent the same procedure without occlusion of the LAD. After LAD ligation, hearts were collected at 24-, 48-, 72-hour, and 1-week. Left ventricles were separated into remote and infarct-at-risk zones for downstream analysis.

Bone marrow monocytes isolation.

Mice were euthanized and the surface is sprayed with the 70% ethanol. The soft tissues were removed from the femurs with a sterile scalpel and the clean bones (n = 4) were transferred into a petri dish on ice. Both ends of the long bone (epiphysis) of the femur were cut to expose the bone marrow (BM). The PBS was used to flush out the bone marrow and collected in a 15 mL tube. The BM cell suspension was centrifuged at 300 g for 5 min, and the pellet was resuspended in cell sorting buffer containing 2% FBS and 1mM EDTA and filtered using a 40μm cell strainer immediately before isolation. We use Fluorescence-activated cell sorting (FACS) method to purify neutrophils. We label the BM single cell suspension with CD45, CD11b, Ly6G, CCR2, and Ly6C. The $CD45^{+}CD11b^{+}Ly6G^{-}$ $Ly6C^{hi}$ cell population (monocytes) is sorted and collected for down stream analysis. In mice with

CCR2-Cre-GFP, the endogeneous GFP is used as a parameter to sort monocytes ($CD45^+CD11b^+Ly6G^-CFP^+$).

Cardiac macrophage isolation.

Cardiac immune cell isolation as performed based on our published protocol[1, 11, 19]. Briefly, The MI tissue were separated from the remote myocardium and rinsed in 4°C PBS. The tissue was extensively rinsed to remove circulating blood followed by mincing with surgery scissors. The minced tissues were then incubated at 37°C for 45 mins in a Thermomixer (Eppendorf) with shaking set at 120rpm in the digestion buffer that contained the following enzymes (all from Sigma, St. Louis, MI): collagenase I (cat. no. SCR103,) 450 unit/mL, hyaluronidase (cat. No. H3884) 60 unit/ml, DNase (cat. 9003-98-9) 60 unit/ml. The tissues were then triturated and passed through a 40 μm strainer. Cells were then washed in 50ml 4°C PBS containing 1% Fetal Calf Serum (FCS) by centrifugation 10 minutes at 400 g. The resulting cell pellet was resuspended in cell sorting buffer before FACS, flow cytometry, or immunomagnetic isolation using the isolation kit from Miltenyi (cat.130-120-337).

Flow cytometry.

The single cell suspension from the infarct tissue, peripheral blood (PB), and bone marrow (BM) was obtained and the cell concentration was adjusted to $1x10^6$/100 μL with sorting buffer. The cells were incubated first with purified anti-mouse CD16/32 (FcBlock) for 10 min at 4 °C followed by adding antibodies to the concentration specified in the table. The cells were incubated with antibodies at 4 °C for 15 min. After the incubation, the cells were pelleted by centrifugation at 500g for 5 minutes and washed two times in the sorting buffer. The labeled cells were subjected to scanning by flow cytometer. Gating strategies are described in the Results section. Mean fluorescence intensity was calculated as the median of the indicated fluorescent parameter using FlowJo software. Cell sorting was performed on an Aria III Fusion (BD Biosciences). No sodium azide in the FACS buffer for sorting experiments. Antibodies used for flow cytometry: from Biolegend: CD45-PE/Cy7 (cat# 103114), CD11b-PB (cat# 101223), F4/80-PE (cat#123109), Ly-6G-APC (cat# 127613), Ly-6C-BV711 (cat# 128037), CD206-PerCP/Cy5.5 (cat# 141715), CD64-FITC (cat# 164405), CCR2-BV421 (cat# 150605).

Preparation of myocardial DAMP (mDAMP).

The remote heart tissue from mice, 3 or 4 days post-myocardial infarction (MI) surgery, was collected for mitochondrial isolation. Briefly, approximately 250 mg of heart tissue was cut into 1–2 mm pieces and rinsed in cold PBS to remove any residual blood. The tissue was then transferred to a homogenizer containing 1 mL of cold MIB (…….) and homogenized on ice. The resulting supernatant

was collected, and the pellet was discarded by centrifugation at 1,000 g for 5 minutes at 4°C. The supernatant was further centrifuged at 12,000 g for 10 minutes at 4°C. The resulting pellet was used as the mitochondrial fraction and subjected to freeze-thaw cycles on dry ice (5 times). sDAMPs were extracted by centrifugation at 12,000 g for 10 minutes and stored at -80°C.

Interstitial fluid extraction from myocardial infarction tissue.

Infarct and remote heart tissues after MI surgery 3 days were collected to extract interstitial fluid by a centrifugation method (Xenia Geeraerts et al. Cell Reports 2021). Briefly, hearts tissue were washed in cold PBS and sectioned into small pieces. 200mg of samples were transferred to an insert with a nylon mesh (20 um opening, 55um thickness, Spetrum Labs) placed on top of a mini spin column (Qiagen) which was removed the bottom filter. The tubes were centrifuged for 15 min at 400g at 4°C and then the insert was removed. The fluid was centrifuged for another 5min art 400g at 4°C. The fluid from 3 samples was pooled and spun for 10min at 4000g at 4°C. The surpernent was stored at -80°C upon proteomic.

Culture to develop Bone marrow-derived macrophages (BMDM)

C57BL6/J female mice, aged 6–8 weeks and weighing 20–25 g, were used to isolate bone marrow cells from their two femurs and two tibias (reference: Gotaro Toda et al., STAR Protocols 2, 100246, March 19, 2021, Preparation and culture of Bone Marrow-Derived Macrophages from Mice for Functional Analysis). Bone marrow cells from one mouse were incubated in 10 mL RPMI-1640 (Bio Life Sciences) supplemented with 10% Fetal Bovine Serum (FBS, Sigma Aldrich), and then filtered through a 40 μm Fisherbrand™ Sterile Cell Strainers (Fisher Scientific). The cells were collected by centrifugation at 300 g for 5 minutes at 4°C and resuspended in RPMI-1640 with 10% FBS and 20 ng/mL recombinant mouse M-CSF (R&D systems). The cells were cultured in two 10-cm Petri dishes at 37°C. After 3–4 days, the culture medium was replaced, and the cells were continued to be cultured until day 6–7. BMDMs were then used for characterization and stimulation experiments.

BMDM Stimulation with sDAMP, EIPA, and NPS

For stimulation, 3×10^5 cells per well were plated in a 12-well plate and cultured overnight at 37°C. The cells were then starved in FBS-free RPMI-1640 for 3 hours. The cells were treated with 100 μg/mL sDAMP protein with or without 12.5 μM 5-n-ethyl-n-isopropyl amiloride (EIPA, Fisher Scientific), 5 μM NPS-2143 (Fisher Scientific), and incubated at 37°C for 3 hours. After the treatment, the cells were collected for protein and RNA extraction.

siRNA-mediated *Slc9a1* silencing.

Slc9a1 in BMDMs were silenced using small interfering RNA (siRNA) (Life Technology Corporation). The sequence sense 5′-CCACAAUUUGACCAACUUAtt-3′ and antisense 5′-UAAGUUGGUCAAAUUGUGGtc-3′ was used to inhibit *Slc9a1* expression and a non-specific sequence sense 5′-UUCUCCGAACGUGUCACGUdTdT-3′and antisense 5′-ACGUGACACGUUCGGAGAAdTdT-3′ were used as a negative control. Cells were transfected with 40 nM *Slc9a1*-targeting or non-targeting control siRNA using Lipofectamine RNAiMAX according to the manufacturer's instructions. Briefly, Cells were seeded at 3×10^5 cells per well in 12-well plates 18–24 hours prior to transfection. For each well, siRNA and Lipofectamine RNAiMAX were diluted separately in Opti-MEM and then combined followed by additional incubation for 5-10 minutes at room temperature to allow complex formation. Complexes were added dropwise to cells with serum-free medium. Medium was replaced to complete medium after 24 hours. Cells were harvested or treated for downstream analysis at 72-96 hours of transfection.

Poly(I:C) and LPS stimulation.

High–molecular weight polyinosinic–polycytidylic acid (Poly(I:C), InvivoGen) and Lipopolysaccharides (LPS, Sigma) were reconstituted in sterile endotoxin-free water at 1 mg/mL. BMDMs were maintained at 37 °C in a humidified incubator containing 5% CO_2 in complete growth medium with 20ng/ml of M-CSF. Cells were seeded 18–24 h prior to stimulation to achieve 70–80% confluence, and the medium was replaced with serum-free medium at the time of treatment. Poly(I:C) or LPS was added directly to the culture medium at a final concentration of 5 ug/ml or 100 ng/mL, respectively. Cells were treated for 4hr and collected for downstream assays.

Rhodamine-Poly(I:C) uptake assay.

Fluorescently labeled Poly(I:C) (Rhodamine-Poly(I:C)), high molecular weight (InvivoGen) was used to assess cellular uptake. BMDMs were seeded at $1–2 \times 10^5$ cells per well in 24-well plates with coverslips and cultured overnight in complete medium at 37°C in 5% CO_2 to allow adherence. Prior to the uptake assay, cells were incubated in serum-free medium to minimize interference from serum components. After incubated with 1 ug/ml of Rhoamine-Poly(I:C) (InvivoGen) at 37°C for 1 h or 4 h, the cells were washed three times with ice-cold PBS to remove unbound ligand and fixed in 2% paraformaldehyde for 15 min at room temperature. Coverslips were mounted with an antifade reagent with DAPI. Images were acquired under identical acquisition settings using confocal microscopy for all groups.

Purification of bone marrow monocytes by FACS.

Bone marrow cells were isolated from 8–12-week-old mice. Femurs and tibias were harvested under sterile conditions. Bone marrow was flushed using a 27-gauge needle with cold sorting buffer (PBS + 0.5 % BSA + 1 mM EDTA). Cell suspensions were passed through a 40-μm cell strainer to obtain single-cell suspensions. Red blood cells were lysed using ACK lysis buffer for 2 minutes at room temperature, followed by washing with sorting buffer. For surface marker staining, cells were incubated with normal Rat serum for 10 minutes at room temperature to prevent nonspecific binding. Cells were then stained for 30 minutes at 4°C under light-free conditions with fluorochrome-conjugated antibodies diluted in sorting buffer. A typical monocyte panel ($CD45^{+}CD11b^{+}Ly6G^{-}GFP^{+}$) were used to select the monocytes from CCR2-CreER-GFP and *Slc9a1*$^{flox/flox}$;CCR2-Cre-GFP mice. After staining, cells were washed resuspended in sorting buffer to perform the cell sorting using the FACS system. The sorted cells were aliquoted for further assays.

In vivo Poly(I:C) and LPS challenge model.

Poly(I:C) and LPS were prepared fresh in sterile saline. EIPA (Thermo Fisher Scientific) was dissolved in DMSO. Wild-type mice were randomly assigned to vehicle or EIPA controls, Poly(I:C) alone, LPS alone, EIPA + Poly(I:C) and EIPA + LPS groups. EIPA was administered subcutaneous (s.c) at 15 mg/kg body weight/day at 1 day and 2 hours prior to Poly(I:C) and LPS challenge. To induce the systemic inflammatory responses, Poly(I:C) or LPS was administered via intraperitoneal (i.p.) injection at 3 mg/kg body weight or 1 mg/kg body weight, respectively. Tissues (spleen, bone marrow, heart) were collected at 4 hours post-injection to perform mRNA analysis by RT-qPCR and protein production detection by western blot assay.

Immunoblot

Harvest cells and lyse cells in RIPA buffer (Fisher Scientific) with protease and phosphatase inhibitors (Protease and Phosphatase Inhibitor Mini Tablets, EDTA-free, Fisher Scientific) and incubate on ice for 15 min. Clarify the lysate by centrifugation at 12,000 x g for 10 minutes at 4°C. Collect the protein sample as supernatant and detect the protein concentration using a BCA protein assay. Dilute the protein sample with 5X loading buffer and heat at 95°C for 5 minutes to denature proteins. Protein lysates were separated by SDS-PAGE, transferred to Hybond-C nitrocellulose membranes and subjected to immunoblot analysis. Incubate the membrane with the primary antibody, gently shaking overnight at 4°C. After incubation, wash the membrane three times for 5 minutes each with TBS-T (tris-buffered saline with 0.1% Tween-20). Incubate the membrane with the IRDye 800CW or 700CW (LICOR) secondary antibody for 1 hour at room temperature with gentle shaking. Wash the membrane again three times for 5 minutes each with TBS-T. Visualize the protein

bands using a LI-COR Odyssey Imaging System and quantify the band intensity using image analysis software of Image Studio.

RNA extraction and RTPCR

Total RNA was extracted from BMDM cells using the Quick-RNA™ Microprep Kit (Zymo Research). Briefly, 1 volume of 95–100% ethanol was added to 1 volume of the sample lysed in RNA Lysis Buffer (1:1). The mixture was then transferred to a Zymo-Spin™ IC Column placed in a Collection Tube and centrifuged. After DNase I treatment, the RNA was washed and eluted from the column using DNase/RNase-Free Water. The RNA was subsequently used in a reverse transcription reaction with PrimeScript™ RT Master Mix (TAKARA) and then analyzed by qPCR using iTaq Universal SYBR Green Supermix (Bio-Rad).

Primers list.

Macropinocytosis assay.

BMDM cells were incubated with a 500 μg/mL solution of dextran 70,000 MW (Oregon Green 488, anionic, lysine-fixable) for 40 min. The cells were then fixed with 4% paraformaldehyde (PFA) for 15 minutes and washed three times with cold PBS. The cell nuclei were stained using Vybrant® DyeCycle™ Violet stain (Invitrogen).

For in vivo dextran uptake investigation, on day 3 after underwent myocardial infarction (MI) surgery, the mice were anesthetized, and the hearts were carefully exposed. A 1 mg/mL solution of dextran 70,000 MW was locally perfused on the surface of the hearts for 30 minutes. The mice were subsequently euthanized, and the hearts were excised immediately above the suture line, then rinsed in ice-cold PBS. The tissues were fixed in 4% PFA at 4°C with gentle shaking for 3 hours. To cryopreserve the heart tissue, it was embedded in OCT compound, snap-frozen in liquid nitrogen, and stored at -80°C.

Lucifer yellow uptake. For fluorescence microscopic observation of macropinosome, BMDM were preincubated for 3 hours in sDAMP solution with or without EIPA, then incubated for 10 min or 30 min in 1.5 mg/ml solution of Lucifer Yellow CH (Thermo fisher scientific), rinsed in PBS, and fixed for 30min in in 4% PFA for 15 min. Then the cell nuclei were stained using Vybrant® DyeCycle ™ Violet stain (Invitrogen).

Histology and Immunohistochemistry

Following euthanasia via cervical dislocation, the animals' hearts were carefully rinsed in PBS and fixed in 4% paraformaldehyde (PFA) at room temperature with gentle agitation. The tissues were then processed for paraffin embedding or Cryo-section using standard protocols. For immunostaining, 5-μm coronal sections were prepared to obtain a four-chamber view of the heart. The sections were permeablilized with 0.25% Triton X-100 in PBS and then blocked with 5% BSA with for 1 hours at room temperature. The primary antibody were applied and incubated overnight. After washing three times with PBS, the sections were incubated with the secondary antibody for 1 hour at room temperature. The sections were then mounted with ProLong™ Gold Antifade Mountant containing DAPI to stain the nucleus. Hematoxylin and eosin (H&E) staining was performed according to standard protocols.

Immunocytochemistry

Cultured BMDM cells were washed three times with PBS, then fixed in 4% PFA for 15 minutes. Cells were permeabilized with 0.1% Triton X-100 for 15 minutes and subsequently blocked in PBS containing 5% BSA for 1 hour. The cells were then incubated with primary antibody. Donkey derived secondary antibodies conjugated to Alexa 488 or 546 were used to visualize the fluorescence signals. ProLong™ Gold Antifade Mountant containing DAPI was used to stain the nucleus.

Live cell imaging method

Time-lapse imaging was used to observe the dynamics of macropinocytosis over time. After starvation in serum free medium for 2 hours, BMDM cells were incubated in 100ug/ml of sDAMP and 1.5 mg/ml of Lucifer yellow solution with or without M-CSF or EIPA for 30min. Using TIR-FM OMX Super Resolution system (Quantitative Light Microscopy Core Facility at UT Southwestern Medical Center), video microscopy captures sequential images at every 30 second intervals. Live cells were maintained in appropriate conditions (37°C, 5% CO2) during imaging.

Single cell RNA sequencing of the macrophages purified from the MI tissue. Single-cell suspensions from infarcted cardiac tissue were generated as previously described[1, 11, 19]. Immune cells were first enriched by positive selection using a CD45 MicroBeads kit according to the manufacturer's instructions (130-052-301, Miltenyi Biotec). The enriched cell fraction was subsequently stained with antibodies against CD45, CD11b, and CD3, and $CD45^{+}CD11b^{+}CD3^{-}$ cells were isolated by fluorescence-activated cell sorting. Sorted cells were assessed for viability (>85%) and immediately processed for single-cell RNA sequencing. Single-cell libraries were prepared using the Chromium Single Cell 3′ Gene Expression platform (10x Genomics) following the manufacturer's protocol. Briefly, single cells were partitioned into nanoliter-scale Gel Bead-in-Emulsions (GEMs),

where cell lysis and barcoded reverse transcription occurred, enabling the incorporation of unique cell barcodes and unique molecular identifiers (UMIs) into cDNA. Following GEM recovery and cDNA amplification, sequencing libraries were constructed and sequenced on an Illumina platform. Raw sequencing data were processed using the Cell Ranger pipeline (10x Genomics) to generate gene-by-cell expression matrices for downstream analysis.

Bone marrow monocye and cardiac macrophage isolation and bulk RNA sequencing.

RNA sequencing was performed by Novogene America (Sacramento, CA). Raw reads of fastq format were firstly processed through in-house perl scripts. In this step, clean data (clean reads) were obtained by removing reads containing adapter, reads containing ploy-N, and low-quality reads from raw data. All the downstream analyses were based on the clean data with high quality. Reference genome (mm10) and gene model annotation files were downloaded from genome website directly. Index of the reference genome was built using Hisat2 v2.0.5 and paired-end clean reads were aligned to the reference genome using Hisat2 v2.0.5. Then, the abundance of each transcript was quantified using feature Counts v1.5.0-p3. Differentially expressed genes (DEGs) analysis was performed using the DEseq2 package, and gene expression was normalized using the relative-log-expression (RLE) in DESeq2.30 Genes with an adjusted P-value <.05 found by DESeq2 were assigned as differentially expressed.

For gene ontology (GO) analysis, metascape (http://metascape.org) was employed to perform gene enrichment and functional annotation analyses in neutrophils with the following ontology sources: Kyoto Encyclopedia of Genes and Genomes (KEGG) Pathway, GO Biological Processes, and Reactome Gene Sets.31 GO terms with corrected P-value <.05 were considered significantly enriched by differential expressed genes. KEGG analysis was used cluster Profiler R package to test the statistical enrichment of differential expression genes in KEGG pathways. For genomic integrity analysis (copy number variation [CNV] analysis) was referred to a previous protocol. Preparation of RNA library and transcriptome sequencing was conducted by Novogene Co., LTD (Beijing, China). Genes with adjusted p-value < 0.05 and $|\log2(\text{FoldChange})| > 0$ were considered as differentially expressed.

Echocardiography.

Mouse echocardiograms were recorded on conscious, gently restrained mice using a Vevo 2100 system and an 18-MHz linear probe as described.23, 56. A short-axis view of the LV at the level of the papillary muscles was obtained, and M-mode recordings were obtained from this view. Left

ventricular internal diameter at end-diastole (LVIDd) and end-systole (LVIDs) were measured from M-mode recordings. Fractional shortening was calculated as (LVIDd − LVIDs)/LVIDd (%).

Statistical analysis.

Findings are expressed as mean ± SD. The data were analyzed using statistical software (GraphPad Prism, version 7.01; GraphPad Software, San Diego, CA). An unpaired Student t test was performed to analyze 2 independent groups. One-way ANOVA coupled with the Tukey post-hoc test was used for pairwise comparisons. In representative datasets, we have also employed nonparametric tests (Wilcoxon rank sum test, Wilcoxon two-sample test, Kruskal-Wallis test). A value of $p < 0.05$ was considered statistically significant and numerical p values are displayed on results.

Results

Macropinocytosis Is Activated in Macrophages in the Infarct Tissue and Pharmacologic Inhibition Attenuates Post-Ischemic Inflammation and Myocardial Injury. By internalize large quantity of soluble content from the environment, macropinocytosis is a process potentially important in delivering DAMP and nutrients in ischemic myocardium critical to macrophage activation and survival. We first determined if MI macrophages have active macropinocytosis. We isolated immune cells from the infarct tissue generated by LAD ligation four days post injury (4-dpi). We incubated these cells with FITC-Dextran 70 (FITC-D70) for thirty minutes. Macropinocytosis is conventionally quantified using high–molecular weight tracers, such as ~70-kDa dextran or comparably sized fluorescent beads, which are preferentially internalized through fluid-phase bulk uptake pathways. Figure 1A depicts the gating strategy of identifying the MI macrophages ($CD45^+CD11b^+Ly6G^-$), neutrophils ($CD45^+CD11b^+Ly6G^+$), and lymphocytes ($CD45^+CD11b^-CD3^+$). As demonstrated in Figure 1B, macrophages are the main cells that engulf FITC-D70. Neutrophils, which are also phagocytes, engulfed D70 to a much lesser extent, whereas lymphocytes showed negligible FITC-D70 uptake. MW of ~70 is the standard used for Next, we devised a model that allowed examining macropinocytosis in vivo by infusing DQ-Red BSA into the infarct tissue for 40 minutes, followed by immediate removal of the heart for cryosection. DQ-Red BSA (67 kDa), a self-quenched fluorescent substrate that emits red fluorescence upon intracellular proteolytic processing, is commonly used as a functional readout of macropinocytic uptake[20]. Figure 1C demonstrated active uptake and degradation of DQ Red BSA mainly in $CD68^+$ macrophages in the infarct region. These data suggest that MI macrophages have a highly robust macropinocytosis and are the major cells with this activity.

Furthermore, we injected EIPA (5-(N-ethyl-N-isopropyl)amiloride), a widely used agent to suppress macropinocytosis, before locally infusing the FITC-D70 into the infarct heart for 40 minutes while keeping the mice on a respirator. The cardiac tissue sections were labeled with macrophage marker CD68. As demonstrated in Figure 1D, the FITC-D70 is readily detectable, and closer examination revealed that all FITC-D70 signals colocalized within $CD68^+$ macrophages (inset in Figure 1D). In mice that were pre-treated with EIPA, the uptake of D70 was diminished (Figure 1D), suggesting EIPA also inhibited macropinocytosis in MI macrophages.

Next, we designed an in vitro system to assess how effective EIPA inhibits macropinocytosis in an environment that simulates what macrophages encounter in the infarct environment. We extracted soluble content using enriched mitochondria preparation from the heart and named the preparation myocardium DAMP (mDAMP). We stimulated BMDM (bone marrow derived macrophage) with mDAMP and DQ-BSA for 40 min in the presence or absence of EIPA and quantified the uptake by measuring “mean intensity”, “integrated intensity”, and “raw intensity” using ImageJ. As demonstrated in Figure 1E and the summarized data in Figures 1F, 1G, and 1H, mDMAP increased the update of DQ-BSA, and EIPA blocked baseline and mDAMP-stimulated DQ-BSA uptake, suggesting it effectively suppressed macropinocytosis in macrophages.

To determine if inhibiting macropinocytosis by EIPA affects myocardial repair, we generated MI model and administered DMSO or EIPA at 12.5 mg/kg/day 24 hours after the MI procedure for a total of three days (Figure 1I). Figure 1J are images of hearts collected from DMSO and EIPA-treated mice 7-dpi. The loss of the conical shape of the LV apex is consistent with more remodeling in DMSO-treated hearts. Consistent with these morphological changes, EIPA treatment reduced the gravimetric indexes of remodeling including heart weight (HW) to tibia length (TL) ratio (Figure 1K), improved EF and FS (Figure 1L and 1M), and decreased LV systolic dimension (Figure 1O).

In aggregates, our data suggest that macropinocytosis is a robustly active process in MI macrophages, and blocking macropinocytosis protects the heart from ischemic injury.

Myocardial DAMP is a strong activator of the TLR4 pathway. Next, we sought to leverage the mDAMP to define the signaling pathways most likely regulated by macropinocytosis in the ischemic environment. To establish the physiological relevance of this approach, we first isolated interstitial fluid from infarcted myocardium (i-IF) collected 48–72 hours after myocardial infarction, a time window during which macrophages are actively exposed to necrosis-derived danger signals in vivo. The DAMP components present in i-IF therefore represent the endogenous molecular environment

encountered by macrophages within the infarct tissue. We then performed comparative proteomic analyses of i-IF and mDAMP. As shown in Figures 2A and 2B, both preparations contained a broad array of known DAMP molecules. Notably, more than 90% of annotated DAMP proteins[21], including established cardiac DAMPs such as myosin[22] and cytochrome C[23], were shared between mDAMP and i-IF. Although the relative abundance of individual proteins varied between the two preparations, their overall DAMP composition was highly conserved. This strong overlap indicates that mDAMP closely recapitulates the endogenous DAMP milieu of the ischemic myocardium and provides a biologically relevant stimulus for interrogating macrophage signaling pathways activated in vivo following myocardial injury.

We next further characterized the signaling properties of the mDAMP. Treatment of BMDMs with mDAMP induced rapid phosphorylation and activation of NF-κB (Supplementary (Suppl) Figures 1A and 1B), as well as immediate and sustained activation of ERK (Supplementary Figures 1C and 1D). In parallel, mDAMP robustly activated mTORC1 signaling, as evidenced by increased phosphorylation of S6 (Supplementary Figure 1E) and hyperphosphorylation of 4EBP1 (Suppl. Figure 1F), which relieves translational repression and reflects enhanced mTORC1 activity. Quantification of mTORC1 activation is summarized in Suppl. Figures 1G and 1H. Notably, similar to ERK, mDAMP-induced mTORC1 activation persisted throughout the experimental time course (Suppl. Figure 1I). The coordinated activation of NF-κB, ERK, and mTORC1 represents a well-established signaling signature of Toll-like receptor (TLR) engagement, particularly downstream of TLR4 ligands[24]. These findings therefore indicate that mDAMP activates macrophages through pathways characteristic of TLR-mediated inflammatory signaling.

The presence of this TLR-activating signature in response to mDAMP suggests that TLR-driven inflammatory signaling plays a dominant role in macrophage activation during acute myocardial ischemia. To link these in vitro observations to the in vivo disease context, we performed RNA sequencing analysis of purified cardiac macrophages isolated from infarcted myocardium and compared them with bone marrow monocytes, the circulating precursors of infarct macrophages, which can also be named as monocyte-derived macrophages (MDM). Strikingly, *Il1b*, a key inflammatory cytokine classically induced downstream of TLR4 signaling, was the most abundantly expressed genes in infarct MDMs. Among major inflammatory mediators implicated in post-MI inflammation, including TNF family members (*Tnfaip2*, *Tnfaip3*, *Tnf*), *Ccl2*, *Il6*, *Il18,* and *Nlrp3*, *Il1b* was the highest expressed cytokine (Figure 2C, blue box). Moreover, *Il1b* expression was increased by approximately 30-fold in infarct MDM compared with bone marrow monocytes (Figure 2D, blue arrow), indicating strong induction by the ischemic tissue environment. Interestingly, even though

prior reports have demonstrated the role of IL1B in aggravating post-MI remodeling and heart failure[25-28], IL1B generated by macrophages in inducing inflammatory injury after MI is an area with surprisingly very limited (if any) data.

Pharmacologic inhibition of macropinocytosis suppresses mDAMP-induced inflammatory response in macrophages. The close compositional similarity between mDAMP and infarct interstitial fluid supports the conclusion that mDAMP functions as a physiologically relevant TLR agonist, recapitulating the endogenous signals that drive TLR-dependent IL1B induction in infarct-associated macrophages. We next determined whether mDAMP directly induces inflammatory cytokine expression in bone marrow–derived macrophages (BMDMs) and whether macropinocytosis plays a role therein. We examined a broad panel of inflammatory mediators, including chemokines of the CCL family (*Ccl2*, *Ccl4*, *Ccl5*), CXCL family (*Cxcl1*, *Cxcl2*, *Cxcl10*), interferons and interferon-stimulated genes (*Ifnb*, *Ifng*, *Irf7*, *Ifit1*, *Ifit3*, *Isg15*, and *Rsad2*), as well as proinflammatory cytokines (*Il1a*, *Il1b*, *Il18*, *Tnfa*, and *Il6*). Among these targets, *Il1b*, *Cxcl10*, and *Il6* were consistently and robustly induced by mDAMP stimulation (Figure 2E), a cytokine profile characteristic of Toll-like receptor-driven inflammatory activation, particularly downstream of TLR4.

Importantly, treatment with EIPA almost completely abrogated mDAMP-induced *Il1b* and *Cxcl10* expression and significantly reduced Il6 induction (Figure 2E). To exclude compound-specific effects, we next tested NPS, a structurally distinct macropinocytosis inhibitor. NPS similarly abolished mDAMP-induced *Il1b* expression (Figure 2F), supporting a necessary role of macropinocytosis in mDAMP-driven macrophage activation. As an additional control, we treated BMDMs with the mitochondria-enriched preparation, named as Myo-DP (myocardium-derived preparation), that we used to extract mDAMP. In contrast to mDAMP, Myo-DP failed to induce inflammatory cytokine expression, including *Il1b*, *Tnfa, Ccl2,* and *Il6* (Suppl Figures 2A-2D), indicating that macrophage activation requires DAMP released from damaged mitochondria/myocardium. Notably, Myo-DP also markedly suppressed LPS-induced cytokine expression (Suppl. Figures 2A-2D) as well as LPS-induced NLRP3, iNOS, and IL1B protein expression (Suppl. Figure 2E). Moreover, Myo-DP blunted TNFA-induced expression of inflammatory cytokines (Suppl. 2F). Taken together, these data demonstrates that inhibiting macropinocytosis efficiently suppressed mDAMP-triggered inflammatory response in macrophage.

Because mDAMP elicits signaling features characteristic of TLR4 activation—including coordinated induction of NF-κB, ERK, mTORC1, and robust Il1b expression—and because both EIPA and NPS markedly suppressed mDAMP-induced Il1b, we reasoned that TLR4 signaling may represent a

principal pathway sensitive to macropinocytosis inhibition. To directly test this possibility, we examined whether macropinocytosis inhibitors attenuate macrophage responses to the canonical TLR4 ligand lipopolysaccharide (LPS). BMDMs were stimulated with LPS (10 ng/ml) in the presence of vehicle, EIPA, or NPS. Both EIPA and NPS markedly blunted LPS-induced expression of *Il1b* and *Cxcl10* (Figure 2G). EIPA precluded IL1B protein expression-induced by LPS (Figures 2H, 2I). Furthermore, EIPA significantly suppressed LPS-induced interferon-stimulated gene (ISG) expression, including *Cxcl10* (Figure 2J), *Ifit1*, *Ifit3*, *Isg15*, *and Rsad2* (Figure 2K). Collectively, these data support a model in which macropinocytosis-dependent processes are required for optimal macrophage responses to both damage-associated molecular patterns and LPS, and that pharmacologic inhibition of macropinocytosis effectively antagonizes TLR4-driven inflammatory signaling.

Deleting *Slc9a1* in monocytes and monocytes-derived macrophages. Given that EIPA-mediated inhibition of macropinocytosis has been largely attributed to suppression of SLC9A1/NHE1 activity, even though EIPA is not a specific inhibitor of SLC9A1, we next employed a macrophage-specific *Slc9a1* deletion strategy to define the contribution of SLC9A1 to the observed inflammatory phenotypes. ~~Although pharmacologic inhibition of macropinocytosis with EIPA has long been attributed to SLC9A1/NHE1 inhibition, recent genetic studies indicate that SLC9A1 is not universally required for macropinocytosis across cell types[17, 29, 30]. This distinction underscores the importance of genetic approaches in defining SLC9A1-specific functions and cautions against equating EIPA sensitivity with SLC9A1 dependence.~~ We first assessed the SLC9A isoform expression in bone marrow (BM) monocytes. RNA sequencing of purified monocytes ($CD45^{+}CD11b^{+}Ly6C^{hi}Ly6G^{-}CD3^{-}$) suggests that *Slc9a1* is the main isoform expressed by monocytes with the highest normalized expression level (Figure 3A). The result is consistent with a prior report that SLC9A1 was the main isoform macrophages expressed. Since the BM monocytes are the precursors of macrophages in the infarct tissue, we therefore proceeded to generate a compound mouse model that carries alleles of Flox (*Slc9a1*$^{fl/fl}$) and the CCR2-CreER-GFP. The *Slc9a1*$^{fl/fl}$ only and CCR2-CreER-GFP only littermates are used as controls. We administered tamoxifen (TMX) at 75 mg/kg body weight for three days to induce *Slc9a1* deletion in monocytes, and the control littermate received the same treatment. After TMX injection, we annotated the *Slc9a1*$^{fl/fl}$;CCR2-CreER-GFP mice as Monocyte(Mon)$^{\Delta Slc9a1}$ and *Slc9a1*$^{fl/fl}$-only or CCR2-CreER-GFP-only mice as Mon$^{Slc9a1\text{-}WT}$. the nomenclature of Mon$^{Slc9a1\text{-}WT}$ and Mon$^{\Delta Slc9a1}$ are inter-changeable with macrophage(Mac)$^{Slc9a\text{-}WT}$ and Mac$^{\Delta Slc9a1}$ when MI models are generated. To confirm SLC9A1 deletion specifically in monocytes, we purified monocytes

($CD45^+CD11b^+Ly6G^-GFP^+$) from the BM and performed immunoblot using protein samples extracted from the purified cells. Figure 2B depicts the gating strategy of monocyte and neutrophil purification. Figure 3C demonstrates the loss of SLC9A1 in GFP^+ monocytes isolated from $Mon^{\Delta Slc9a1}$ mice compared to the GFP^+ monocytes from CCR2-CreER-GFP only mice.

Cardiac Immune phenotyping of $Mac^{Slc9a\text{-}WT}$ and $Mac^{\Delta Slc9a1}$ mice after MI. To determine whether macrophage-specific deletion of *Slc9a1* alters myeloid cell dynamics following MI, we performed flow cytometric analysis of infarct tissue at 3- and 7-dpi. As illustrated in Figures 4A-4D, we profiled four principal myeloid populations: (1) total macrophages ($CD45^+CD11b^+Ly6G^-$); (2) GFP^+ MDMs ($CD45^+CD11b^+Ly6G^-GFP^+$); (3) recently recruited inflammatory monocytes ($CD45^+CD11b^+Ly6G^-GFP^+Ly6C^{hi}$); and (4) neutrophils ($CD45^+CD11b^+Ly6G^+Ly6C^{int}GFP^-$). At 3-dpi, deletion of *Slc9a1* resulted in a significant reduction in total macrophages, GFP^+ MDMs, and newly recruited $Ly6C^{hi}$ inflammatory monocytes within the infarcted myocardium (Figures 4E-4G). In contrast, neutrophil numbers were modestly increased in $Mac^{\Delta Slc9a1}$ mice at this early time point (Figure 4H). By 7-dpi, however, the numbers of neutrophils, $Ly6C^{hi}$ monocytes, and GFP^+ MDMs were comparable between control and knockout cohorts (Figures 4I-4L).These findings indicate that conditional deletion of *Slc9a1* transiently impairs early monocyte recruitment and MDM accumulation following MI, particularly during the acute inflammatory phase, but does not produce sustained alterations in myeloid cell composition at later stages of remodeling.

Macrophage-specific *Slc9a1* deletion protects the heart from acute ischemia. To determine if deleting *Slc9a1* in MI macrophages recapitulates the cardiac protection from EIPA, we generated myocardial infarction model by performing LAD (left anterior descending artery) ligation in macrophage(Mac)$^{\Delta Slc9a1}$ and $Mac^{Slc9a1\text{-}WT}$ mouse cohorts. As the MI macrophages are exclusively derived from circulating $CCR2^+$ monocytes, using the CCR2-Cre will result conditional *Slc9a1* deletion in the monocyte-derived macrophages (MDM) in MI. One week after the MI procedure (7 dpi), we measured cardiac function, left ventricular dimensions, and the gravimetric parameter HW/TL as markers of ischemia-induced cardiac remodeling. Figure 2D demonstrates that deleting *Slc9a1* in MDMs decreased cardiac mass as indicated by lower HW/TL compared to the control mice. We also observed better cardiac function (fraction shortening (FS), Figure 2E) and smaller left ventricle systolic dimensions (LVID;s) in the $Mac^{\Delta Slc9a1}$ cohort (Figure 2F). Figure 2H shows representative serial cross-sections illustrating the extent of scar formation following MI in $Mac^{\Delta Slc9a1}$

and Mac$^{Slc9a1\text{-WT}}$ mice. Scar length was quantified as a reliable indicator of left ventricular (LV) remodeling after MI[1, 11], and a remodeling index (RI) was calculated as the ratio of LV internal diameter to septal thickness. As summarized in Figures 2I and 2J, monocyte-derived macrophage (MDM)–specific deletion of *Slc9a1* significantly reduced scar size and decreased the RI. Collectively, these findings indicate that SLC9A1 in MDMs promotes adverse post-MI remodeling and contributes to impaired cardiac function.

SLC9A1 promotes type I interferon pathway activation in monocyte-derived macrophages of the MI. To elucidate the mechanisms by which SLC9A1 MDM function after MI, we purified myeloid cells (CD45$^+$CD11b$^+$) from infarcted hearts at 4 dpi and subjected them to single-cell RNA sequencing using the 10x Genomics platform. Unsupervised clustering identified eight distinct cell populations, including four macrophage clusters (Mac1-Mac4), neutrophils, dendritic cell-like (DC-like) cells, a small population of Mki67$^+$ proliferating cells, and rare lymphocytes (Figure 5A). Canonical marker genes for each cluster are shown in Figure 5B. We focused subsequent analyses on the macrophage populations.

The *Flt1*$^+$*Trem2*$^+$*Lgmn*$^+$*Ms4a7*$^+$*Ctsb*$^+$ cluster (Mac1) exhibited a transcriptional signature consistent with reparative, efferocytosis-enriched macrophages. Genes such as *Lgmn*, *Trem2*, and *Ctsb* are associated with phagocytic clearance and resolution of inflammation[31, 32], while *Trem2* also mediates lipid sensing and resolution programs[32, 33]. Expression of *Flt1* (*Vegfr1*) suggests potential involvement in angiogenic or VEGF-related signaling. The enrichment of efferocytosis-associated and pro-resolution pathways indicates that Mac1 likely represents emerging reparative, M2-like macrophages that arise during the second half of the first week following MI. Consistent with this interpretation, *Ms4a7* has been implicated in promoting M2-like polarization and immune suppression[34].

The *Gm26917*$^+$*Neat1*$^+$*Cdk8*$^+$*Camk1d*$^+$ cluster (Mac2) displayed a transcriptional profile indicative of interferon and NFKB pathway activation. Both *Neat1* and *Gm26917* are long noncoding RNAs associated with inflammasome activation and TLR/NFKB–mediated inflammatory responses[34, 35]. CDK8 encodes a transcriptional kinase that amplifies IFN- and NFKB-dependent gene programs, while *Camk1d* suggests Ca^{2+}-dependent pro-inflammatory signaling[36, 37]. Together, these features define Mac2 as a strongly pro-inflammatory macrophage population.

The *Ms4a4c*$^+$*Plac8*$^+$*Vcan*$^+$*Ifitm3*$^+$*Ly6c2*$^+$ cluster (Mac3) likely represents recently recruited monocyte-derived macrophages in the injured heart. High expression of *Ly6c2* and *Plac8* reflects monocyte-associated signatures[38], while *Vcan* indicates engagement with extracellular matrix and vascular

interfaces. The presence of the interferon-stimulated gene *Ifitm3* further supports an activated, newly infiltrating phenotype. This profile is consistent with prior single-cell studies of muscle and nerve injury in which Plac8 and Ifitm3 marked infiltrating and activated monocyte–macrophage subsets[39].

Finally, the Mac4 cluster was characterized by expression of *Lyve1*, a marker of tissue-resident macrophages, and enrichment of *Mgl2* (*CD301b*), commonly associated with resident, M2-like macrophages[40]. These features suggest that Mac4 represents cardiac resident macrophages. The presence of this population likely reflects inclusion of border-zone myocardium during cell isolation, despite efforts to enrich primarily for infarct tissue. The proportion of each cluster is depicted in Figure 5C.

SLC9A1 promotes interferon stimulated gene response in MI. Using the scRNA-seq dataset, we performed differentially expressed gene (DEG) analysis comparing the main macrophage clusters (Mac1,2,3) between Mac$^{\Delta Slc9a1}$ and Mac$^{Slc9a1\text{-WT}}$ mice. Strikingly, interferon-stimulated genes (ISGs) emerged as the predominant transcriptional program downregulated upon deletion of *Slc9a1*. Among the top 20 most significantly downregulated genes, approximately 80% were ISGs. Figure 5D illustrates the expression of 46 ISGs identified within the top 100 differentially expressed genes across the Mac1, Mac2, and Mac3 clusters. Deletion of *Slc9a1* resulted in broad suppression of these ISGs across macrophage subsets. Notably, macrophages within the Mac3 cluster exhibited the highest baseline expression of ISGs compared to Mac1 and Mac2. This cluster likely corresponds to the previously described IFN cardiac macrophage population[2]. Consistent with this interpretation, Mac3 cells display features of recently recruited monocyte-derived macrophages, including high expression of *Ly6c2*, aligning with prior reports that post-MI ISG responses are initiated in the bone marrow[41]. Representative UMAP heatmaps (Figure 5E) further demonstrate reduced expression of canonical ISGs, including *Isg15* and *Irf7*, in *Slc9a1*-deficient macrophages compared with wild-type controls.

Gene Set Enrichment Analysis (GSEA) confirmed these observations. The most significantly enriched pathway among downregulated genes was the Hallmark IFNA response signature (Figure 5F). Consistently, Gene Ontology (GO) analysis revealed enrichment of pathways related to defense response to virus, type I interferon production, and innate immune activation (Figure 5G), supporting a central role for SLC9A1 in regulating interferon-driven inflammatory programs.

To independently validate the reduction in type I interferon signaling, we performed quantitative RT-PCR on RNA isolated from infarct tissue of Mac$^{\Delta Slc9a1}$ and Mac$^{Slc9a1\text{-WT}}$ mice. As shown in Figures 5H-

5L, macrophage-specific deletion of *Slc9a1* significantly reduced expression of key ISGs, including *Cxcl10*, *Ifit3*, *Irf7*, *Isg15*, and *Rsad2*. These findings corroborate the single-cell RNA-sequencing results and establish SLC9A1 as a critical promoter of type I interferon pathway activation in infarct-associated macrophages.

SLC9A1 Enhances Interferon Responses by Facilitating TLR3 Signaling. To define the mechanism by which SLC9A1 regulates type I interferon (IFN) and ISG responses, we focused on the principal endosome-dependent signaling pathways linking endocytosis to IFN induction - namely TLR3 and TLR4. TLR3 recognizes double-stranded RNA mimetics such as Poly(I:C), whereas TLR4 is activated by lipopolysaccharide (LPS). Engagement of these receptors triggers NFKB activation and, following ligand or ligand-receptor internalization, IRF3-dependent signaling that drives expression of ISGs and inflammatory cytokines (e.g., *Il1b*, *Il6*)[42].

To directly assess the role of SLC9A1, we performed siRNA-mediated knockdown in BMDMs using a validated and previously published siRNA sequence (ref). Efficient reduction of SLC9A1 protein levels was confirmed by immunoblotting (Figure 6A). Macrophages were then stimulated with free poly(I:C) (without transfection reagents) to selectively engage endosomal TLR3 signaling. As shown in Figures 6B–6F, *Slc9a1* knockdown significantly reduced Poly(I:C)-induced expression of ISGs, including *Cxcl10*, *Ifit1*, and *Isg15*, as well as inflammatory cytokines *Il1b* and *Il6*. In contrast, *Irf7* expression was not significantly affected (Figure 6G). These findings indicate that SLC9A1 facilitates TLR3-dependent inflammatory and ISG responses.

To extend these observations in vivo, we administered Poly(I:C) intraperitoneally (5 µg/g body weight) to Mon$^{\Delta Slc9a1}$ mice and control littermate controls (Mon$^{Slc9a1\text{-WT}}$). Bone marrow monocytes ($CD45^+CD11b^+GFP^+$) were isolated four hours after injection to assess activation of the TLR3–IFN–ISG axis. As shown in Figures 6H-6L, Slc9a1-deficient monocytes exhibited significantly attenuated induction of *Cxcl10*, *Ifit1*, *Ifit3*, *Isg15*, and *Rsad2* compared with controls. Collectively, these in vitro and in vivo data demonstrate that SLC9A1 promotes TLR3-mediated interferon signaling and supports a broader role for SLC9A1 in regulating endosome-dependent innate immune pathways.

SLC9A1 Has Limited Impact on Cytosolic Nucleic acid Receptor-Mediated IFN–ISG Activation. In addition to endosomal TLR3, double-stranded RNA (dsRNA) such as Poly(I:C) can be detected in the cytosol by the RNA sensors IFIH1 (MDA5) and RIG-I, leading to robust activation of the TBK1–

IRF3 axis and subsequent induction of type I interferon and ISGs. To determine whether SLC9A1 also regulates IFIH1/RIG-I–dependent signaling, we delivered Poly(I:C) directly into the cytosol by transfection following siRNA-mediated knockdown of Slc9a1 in BMDMs. As expected, transfected Poly(I:C) induced strong phosphorylation of TBK1 and IRF3, confirming activation of the cytosolic RNA-sensing pathway (Figure 6M). In contrast to stimulation with free poly(I:C), which requires endosomal uptake, knockdown of *Slc9a1* did not significantly attenuate TBK1 or IRF3 phosphorylation in response to cytosolic Poly(I:C). Consistently, expression of representative ISGs, including *Cxcl10*, *Ifit1*, and *Irf7*, was not reduced following Poly(I:C) transfection in *Slc9a1*-deficient macrophages (Figures 6N-6P). These findings indicate that SLC9A1 selectively facilitates endosome-dependent TLR3 signaling but does not substantially regulate cytosolic RNA sensor–mediated IFN–ISG activation.

SLC9A1 Promotes TLR3 Signaling by Regulating Poly(I:C) Endocytosis. Extracellular poly(I:C) is internalized through receptor-mediated endocytic pathways, including uptake via scavenger receptors[43, 44]. To determine whether SLC9A1 regulates this process, we tracked the internalization of rhodamine-labeled Poly(I:C) (Rho-Poly(I:C)) in BMDMs. As shown in Figure 6Q, Rho-Poly(I:C) was efficiently internalized by control macrophages. In contrast, knockdown of *Slc9a1* reduced intracellular Rho-Poly(I:C) accumulation. Quantitative image analysis using standardized thresholding (ImageJ, see Methods) demonstrated a significant reduction in the proportion of cells exceeding the fluorescence threshold (Figure 6R), as well as decreases in mean fluorescence intensity, integrated intensity, and raw fluorescence intensity in Slc9a1-deficient macrophages (Figures 6S-6U).

To further assess endocytic trafficking, we examined early endosome formation by immunostaining for the early endosomal marker EEA1 (Figure 6V). Under basal conditions, no significant differences were observed between control and *Slc9a1*-deficient macrophages in the percentage of $EEA1^+$ cells. Poly(I:C) stimulation increased early endosome formation (Figure 6W), and *Slc9a1* knockdown significantly reduced early endosome formation (Figure 6W). Consistently, mean, integrated, and raw EEA1 fluorescence intensities were all diminished in *Slc9a1*-deficient macrophages after poly(I:C) exposure (Figures 6X-6Z).

Collectively, the impaired uptake of Rho-poly(I:C) and the reduction in early endosome formation in *Slc9a1*-deficient macrophages support a model in which SLC9A1 facilitates endocytic trafficking required for efficient endosome-dependent TLR3 activation.

Pharmacologic SLC9A Inhibition Mitigates TLR-Induced Cardiac Inflammation In Vivo. Having established that SLC9A1 facilitates TLR3-dependent signaling, we next examined whether macrophage *Slc9a1* knockdown similarly modulates TLR4 activation. BMDMs were stimulated with LPS (10 ng/mL) following treatment with control siNC or si*Slc9a1*. As demonstrated earlier (Figure 2), the SLC9A inhibitor EIPA robustly suppressed LPS-induced inflammatory responses, reducing *Il1b* expression by approximately 80% and markedly attenuating ISG induction. In contrast, *Slc9a1* knockdown exerted only a selective effect on LPS-triggered gene expression. While expression of *Cxcl10* and *Il6* was significantly reduced, other key targets, including *Il1b*, *Ifit1*, *Isg15*, and *Rsad2*, were largely unaffected (Figures 7A-7D). These findings indicate that genetic disruption of *Slc9a1* does not fully recapitulate the broad anti-inflammatory effects observed with EIPA. Rather, SLC9A1 appears to play a more selective role in macrophage signaling, whereas pharmacologic SLC9A inhibition exerts wider effects on TLR4-driven inflammatory activation.

We next examined the translational relevance of pharmacologic SLC9A inhibition in vivo. Mice were systemically challenged with LPS or Poly(I:C) and co-treated with vehicle or EIPA. Notably, the heart mounted a more robust inflammatory response to both TLR 3 and 4 ligands compared with bone marrow and spleen (Figures 7E and 7L). EIPA treatment significantly attenuated LPS-induced cardiac inflammation, reducing expression of ISGs (*Cxcl10*, *Ifit1*, *Ifit3, Isg15*, *Rsad2*) and inflammatory cytokines such as *Il1b* and *Tnfa*. Similarly, in Poly(I:C)-challenged mice, EIPA suppressed cardiac expression of ISGs (*Cxcl10*, *Ifit1*, *Ifit3, Irf7*, *Isg15*, *Rsad2*) and the cytokine *Il6* (Figure 7M-7T).

Collectively, these results demonstrate that pharmacologic SLC9A inhibition effectively mitigates TLR3- and TLR4-driven cardiac inflammation in vivo. While genetic deletion reveals a selective role for SLC9A1 in endosome-dependent interferon signaling, pharmacologic inhibition exerts broader anti-inflammatory effects, highlighting the therapeutic potential of targeting endocytic-dependent innate immune activation in inflammatory cardiac injury by an existing clinical drug.

Discussion

In this study, we sought to define the role of macropinocytosis in macrophages during post-MI repair and remodeling. We demonstrate that macropinocytosis is robustly activated in the infarcted heart and that MI-associated macrophages represent the predominant macropinocytic population. Pharmacologic inhibition of this process with the amiloride derivative EIPA conferred significant protection against ischemic injury, improving cardiac function and attenuating adverse remodeling. To define the macrophage-intrinsic mechanisms underlying these effects, we generated monocyte-

and monocyte-derived macrophage (MDM)-specific deletion of *Slc9a1*, the predominant Na^+/H^+ exchanger isoform expressed in these cells and a principal molecular target of EIPA. Conditional deletion of *Slc9a1* phenocopied the cardioprotective effects observed with EIPA treatment, establishing an important role for macrophage SLC9A1 in ischemic injury responses.

Mechanistically, loss of *Slc9a1* markedly suppressed interferon-stimulated gene (ISG) expression in monocytes and MDMs. Using complementary in vitro and in vivo approaches, we demonstrate that SLC9A1 facilitates TLR3-dependent signaling by promoting ligand endocytosis and delivery to endosomal signaling compartments. Notably, genetic deletion of *Slc9a1* did not fully recapitulate the inhibitory effects of EIPA on TLR4 signaling, indicating that pharmacologic SLC9A inhibition extends beyond selective SLC9A1 blockade. EIPA robustly suppressed cardiac inflammatory responses induced by systemic Poly(I:C) and LPS, extending the relevance of our findings beyond sterile ischemic injury to inflammatory states associated with viral and bacterial triggers. These findings reveal a previously unrecognized divergence between genetic SLC9A1 deletion and pharmacologic NHE inhibition in the regulation of TLR3 and TLR4 signaling. While macrophage SLC9A1 functions as a selective modulator of endosome-dependent innate immune activation, pharmacologic SLC9A inhibition exerts broader anti-inflammatory effects. Together, these results suggest that both SLC9A1-specific strategies and more global SLC9A inhibition may hold therapeutic potential in myocardial injury, systemic infection, and inflammation-driven cardiac dysfunction.

Macropinocytosis as a Checkpoint of Inflammatory Sensing. Macrophages are among the most plastic cells, and their phenotypes are decided through an interplay between changes in their transcriptional programs and environmental cues[8, 9]. In the infarcted myocardium, where large quantities of DAMPs are released, macropinocytosis provides an efficient mechanism to internalize and concentrate these signals. As macropinosomes mature and integrate into the endosomal system, they generate signaling-competent compartments that facilitate interactions between DAMPs and PRRs, thereby promoting activation of the NFKB and IRF3 pathways, leading to the inflammatory cytokine and chemokine expression to exacerbate ischemic injury.

We further show that myocardial DAMP preparations closely recapitulate the endogenous ischemic milieu and elicit signaling profiles characteristic of TLR4 activation. Inhibition of macropinocytosis attenuated these responses, supporting the concept that macropinocytosis functions as an upstream checkpoint governing DAMP-induced inflammatory amplification. These findings identify macropinocytosis as an essential regulator of TLR4-dependent inflammatory signaling in the injured heart.

Divergent Effects of Genetic SLC9A1 Deletion and Pharmacologic Inhibition. EIPA's primary mechanism of action is the inhibition of the plasma membrane Na^+/H^+ exchanger (SLC9A/NHE), particularly SLC9A1 because of its high affinity to this isoform (IC50 0.01 to 0.02 μM), which are 8 to thousands-fold lower than the IC50s of other SLC9As[45]. Together with the evidence that SLC9A1 is the main isoform expressed by monocytes and MDMs, it is expected that EIPA, which is the "gold standard"/selective pharmacologic tool to gauge macropinocytosis, functions via SLC9A1 to inhibit macropinocytosis. However, our data indicate a differential effects of genetic *Slc9a1* knockdown and deletion versus pharmacologic inhibition with EIPA on TLR3 and TLR4 signaling. This likely reflects the distinct mechanistic requirements of these pathways and the broader cellular actions of EIPA. Genetic deletion or siRNA-mediated knockdown of Slc9a1 most prominently impaired TLR3 signaling, consistent with the obligate dependence of TLR3 on ligand internalization and endosomal access. Because TLR3 signals exclusively from intracellular compartments, any reduction in SLC9A1-dependent membrane dynamics, endocytic flux, or endosomal delivery of Poly(I:C) would be expected to disproportionately suppress TLR3 activation.

In contrast, pharmacologic inhibition with EIPA attenuated both Poly(I:C)-TLR3 and LPS-TLR4 signaling while also suppressing TLR3 responses. Unlike genetic deletion, EIPA exerts broader effects on membrane dynamics, intracellular pH regulation, and endocytic trafficking. These broader perturbations likely interfere with CD14-dependent TLR4 internalization and adaptor switching required for TRIF-mediated endosomal signaling. Thus, EIPA disrupts membrane trafficking processes that are critical for TLR4 activation, whereas SLC9A1 more selectively supports TLR3-dependent endosomal signaling.

Together, these findings support a model in which SLC9A1 plays a specific role in enabling efficient endosomal delivery of extracellular RNA ligands, while pharmacologic SLC9A inhibition broadly suppresses membrane remodeling and trafficking processes. This distinction explains the overlapping yet non-identical effects of genetic and pharmacologic perturbations and underscores the importance of genetic approaches in defining isoform-specific immune functions.

SLC9A1 in Endocytic Regulation. The finding of SLC9A1 selectively promotes the uptake of TLR3 ligands is intriguing as it implies the role of SLC9A1 in receptor-mediated endocytosis, the currently known path that delivers the ligand to the endosomal receptor TLR3[43, 44]. Although there is no strong evidence that SLC9A1 directly regulates canonical receptor-mediated endocytosis machinery (e.g., clathrin, AP2, dynamin, Rab5/7) by binding to or modifying those components, SLC9A1 regulates key biophysical prerequisites of receptor-mediated endocytosis, including submembranous pH[30] and

actin dynamics[13], thereby shaping membrane remodeling processes membrane curvature and cortical tension required for efficient endocytic uptake[46,47]. In macrophages, where rapid ligand uptake and endosomal signaling are central to innate immune activation, SLC9A1-dependent control of membrane dynamics may therefore regulate the efficiency with which TLR3 ligands, such as extracellular RNA are internalized and delivered to signaling-competent endosomal compartments. Additionally, it is also possible that the TLR3 ligands are internalized via the non-selective fluid phase uptake (macropinocytosis), a process that SLC9A1 is conducive and generates macropinosomes, which eventually deliver their contents to endo-lysosomes. However, how SLC9A1 selectively engages with the TLR3 ligand endocytosis process remains to be elucidated in future studies.

Translational Implications of SLC9A Inhibition. To assess translational relevance, we evaluated the effects of pharmacologic NHE inhibition in models of systemic innate immune activation. Despite limited isoform specificity, amiloride derivatives markedly attenuated cardiac inflammation induced by systemic poly(I:C) and LPS. From a clinical perspective, therapeutic benefit may not require strict isoform specificity if modulation of dominant membrane-trafficking pathways is sufficient to suppress maladaptive inflammation.

In our short-duration systemic LPS and poly(I:C) challenge models, the robust attenuation of cardiac inflammatory responses by EIPA occurred within a timeframe in which substantial recruitment of circulating immune cells to the myocardium is unlikely. Notably, the heart exhibited a more pronounced inflammatory response to these TLR ligands than immune cell-rich organs such as bone marrow and spleen. These observations raise the possibility that EIPA exerts anti-inflammatory and antiviral effects not only through modulation of monocyte-macrophage function but also through direct actions on resident cardiac cell populations, including cardiomyocytes. Given that cardiomyocytes express functional TLRs and contribute to inflammatory signaling during systemic infection, further investigation into the cell-type–specific effects of SLC9A inhibition is warranted. Such studies may be particularly relevant in conditions such as sepsis-induced cardiomyopathy, where excessive innate immune activation within the myocardium contributes to cardiac dysfunction.

Limitations. Several limitations warrant consideration. First, although we establish a functional link between SLC9A1 and TLR3-dependent signaling, the precise molecular mechanism by which SLC9A1 regulates ligand endocytosis and endosomal signaling remains to be defined. Second, our study focused on the monocyte–macrophage compartment; the potential contributions of SLC9A1 in other cardiac cell types, including cardiomyocytes, were not addressed.

Conclusion. In summary, our study identifies macrophage SLC9A1 as a previously unrecognized regulator of innate immune activation in the injured heart. By facilitating endocytic processes required for TLR3-dependent signaling, SLC9A1 amplifies interferon-driven inflammatory responses that contribute to post–myocardial infarction remodeling. The differential effects observed between genetic Slc9a1 deletion and pharmacologic inhibition underscore the complexity of membrane trafficking and ion exchange in shaping innate immune signaling pathways. Importantly, we demonstrate that EIPA, an amiloride derivative with established clinical use, exerts potent anti-inflammatory effects in the heart in response to TLR3 and TLR4 activation, revealing unexpected translational potential. Together, these findings expand the conceptual framework linking Na^+/H^+ exchange, membrane dynamics, and endosome-dependent immune signaling, and provide a foundation for future therapeutic strategies targeting SLC9A-dependent pathways to modulate inflammation in myocardial injury and systemic inflammatory states.

Reference Cited.

1. Cao DJ, Schiattarella GG, Villalobos E, Jiang N, May HI, Li T, Chen ZJ, Gillette TG and Hill JA. Cytosolic DNA Sensing Promotes Macrophage Transformation and Governs Myocardial Ischemic Injury. *Circulation*. 2018;137:2613-2634.

2. King KR, Aguirre AD, Ye YX, Sun Y, Roh JD, Ng RP, Jr., Kohler RH, Arlauckas SP, Iwamoto Y, Savol A, Sadreyev RI, Kelly M, Fitzgibbons TP, Fitzgerald KA, Mitchison T, Libby P, Nahrendorf M and Weissleder R. IRF3 and type I interferons fuel a fatal response to myocardial infarction. *Nat Med*. 2017;23:1481-1487.

3. Commisso C, Davidson SM, Soydaner-Azeloglu RG, Parker SJ, Kamphorst JJ, Hackett S, Grabocka E, Nofal M, Drebin JA, Thompson CB, Rabinowitz JD, Metallo CM, Vander Heiden MG and Bar-Sagi D. Macropinocytosis of protein is an amino acid supply route in Ras-transformed cells. *Nature*. 2013;497:633-7.

4. Condon ND, Heddleston JM, Chew TL, Luo L, McPherson PS, Ioannou MS, Hodgson L, Stow JL and Wall AA. Macropinosome formation by tent pole ruffling in macrophages. *J Cell Biol*. 2018;217:3873-3885.

5. Jayashankar V and Edinger AL. Macropinocytosis confers resistance to therapies targeting cancer anabolism. *Nature Communications*. 2020;11:1121.

6. Kay RR. Macropinocytosis: Biology and mechanisms. *Cells & Development*. 2021;168:203713.

7. Wei Y, Li W, Xu R, Xu C, Li X, Li N, Xu F, Yang K and Yuan B. Multivalent Co-assembly of LL37-CpG nanoparticles: Enhanced immune response through activating multiple cell internalization pathways. *Mater Today Bio*. 2025;33:102011.

8. Masuda T, Sankowski R, Staszewski O, Böttcher C, Amann L, Sagar, Scheiwe C, Nessler S, Kunz P, van Loo G, Coenen VA, Reinacher PC, Michel A, Sure U, Gold R, Grün D, Priller J, Stadelmann C and Prinz M. Spatial and temporal heterogeneity of mouse and human microglia at single-cell resolution. *Nature*. 2019;566:388-392.

9. Van Hove H, Martens L, Scheyltjens I, De Vlaminck K, Pombo Antunes AR, De Prijck S, Vandamme N, De Schepper S, Van Isterdael G, Scott CL, Aerts J, Berx G, Boeckxstaens GE, Vandenbroucke RE, Vereecke L, Moechars D, Guilliams M, Van Ginderachter JA, Saeys Y and Movahedi K. A single-cell atlas of mouse brain macrophages reveals unique transcriptional identities shaped by ontogeny and tissue environment. *Nat Neurosci*. 2019;22:1021-1035.

10. Steinman RM, Brodie SE and Cohn ZA. Membrane flow during pinocytosis. A stereologic analysis. *Journal of Cell Biology*. 1976;68:665-687.

11. Chen G, Phan V, Luo X and Cao DJ. The mechanistic target of rapamycin complex 1 critically regulates the function of mononuclear phagocytes and promotes cardiac remodeling in acute ischemia. *J Mol Cell Cardiol*. 2021;159:62-79.

12. Counillon L, Bouret Y, Marchiq I and Pouysségur J. Na+/H+ antiporter (NHE1) and lactate/H+ symporters (MCTs) in pH homeostasis and cancer metabolism. *Biochimica et Biophysica Acta (BBA) - Molecular Cell Research*. 2016;1863:2465-2480.

13. Denker SP, Huang DC, Orlowski J, Furthmayr H and Barber DL. Direct Binding of the Na–H Exchanger NHE1 to ERM Proteins Regulates the Cortical Cytoskeleton and Cell Shape Independently of H+ Translocation. *Molecular Cell*. 2000;6:1425-1436.

14. Wu KL, Khan S, Lakhe-Reddy S, Jarad G, Mukherjee A, Obejero-Paz CA, Konieczkowski M, Sedor JR and Schelling JR. The NHE1 Na+/H+ exchanger recruits ezrin/radixin/moesin proteins to regulate Akt-dependent cell survival. *J Biol Chem*. 2004;279:26280-6.

15. Canton J, Schlam D, Breuer C, Gütschow M, Glogauer M and Grinstein S. Calcium-sensing receptors signal constitutive macropinocytosis and facilitate the uptake of NOD2 ligands in macrophages. *Nat Commun*. 2016;7:11284.

16. Beesetty P, Rockwood J, Kaitsuka T, Zhelay T, Hourani S, Matsushita M and Kozak JA. Phagocytic activity of splenic macrophages is enhanced and accompanied by cytosolic alkalinization in TRPM7 kinase-dead mice. *The FEBS Journal*. 2021;288:3585-3601.

17. Lin HP, Singla B, Ahn W, Ghoshal P, Blahove M, Cherian-Shaw M, Chen A, Haller A, Hui DY, Dong K, Zhou J, White J, Stranahan AM, Jasztal A, Lucas R, Stansfield BK, Fulton D, Chlopicki S and Csányi G. Receptor-independent fluid-phase macropinocytosis promotes arterial foam cell formation and atherosclerosis. *Sci Transl Med*. 2022;14:eadd2376.

18. Liu C-L, Zhang X, Liu J, Wang Y, Sukhova GK, Wojtkiewicz GR, Liu T, Tang R, Achilefu S, Nahrendorf M, Libby P, Guo J, Zhang J-Y and Shi G-P. Na+-H+ exchanger 1 determines atherosclerotic lesion acidification and promotes atherogenesis. *Nature Communications*. 2019;10:3978.

19. Zhu J, Ruan X, Mangione MC, Parra P, Chen G, Su X, Luo X and Cao DJ. The cGAS-STING pathway promotes acute ischemia-induced neutropoiesis and neutrophil priming in the bone marrow. *Basic Res Cardiol*. 2025;120:677-705.

20. Commisso C, Davidson SM, Soydaner-Azeloglu RG, Parker SJ, Kamphorst JJ, Hackett S, Grabocka E, Nofal M, Drebin JA, Thompson CB, Rabinowitz JD, Metallo CM, Vander Heiden MG and Bar-Sagi D. Macropinocytosis of protein is an amino acid supply route in Ras-transformed cells. *Nature*. 2013;497:633-637.

21. Roh JS and Sohn DH. Damage-Associated Molecular Patterns in Inflammatory Diseases. *Immune Netw*. 2018;18:e27.

22. Zhang P, Cox CJ, Alvarez KM and Cunningham MW. Cutting edge: cardiac myosin activates innate immune responses through TLRs. *J Immunol*. 2009;183:27-31.

23. Wenzel TJ, Bajwa E and Klegeris A. Cytochrome c can be released into extracellular space and modulate functions of human astrocytes in a toll-like receptor 4-dependent manner. *Biochimica et Biophysica Acta (BBA) - General Subjects*. 2019;1863:129400.

24. Ribeiro MC, Peruchetti DB, Silva LS, Silva-Filho JL, Souza MC, Henriques MDG, Caruso-Neves C and Pinheiro AAS. LPS Induces mTORC1 and mTORC2 Activation During Monocyte Adhesion. *Front Mol Biosci*. 2018;5:67.

25. Toldo S, Mezzaroma E, Van Tassell BW, Farkas D, Marchetti C, Voelkel NF and Abbate A. Interleukin-1β blockade improves cardiac remodelling after myocardial infarction without interrupting the inflammasome in the mouse. *Exp Physiol*. 2013;98:734-45.

26. Mezzaroma E, Toldo S, Farkas D, Seropian IM, Van Tassell BW, Salloum FN, Kannan HR, Menna AC, Voelkel NF and Abbate A. The inflammasome promotes adverse cardiac remodeling following acute myocardial infarction in the mouse. *Proc Natl Acad Sci U S A*. 2011;108:19725-30.

27. Bujak M, Dobaczewski M, Chatila K, Mendoza LH, Li N, Reddy A and Frangogiannis NG. Interleukin-1 receptor type I signaling critically regulates infarct healing and cardiac remodeling. *Am J Pathol*. 2008;173:57-67.

28. Louwe MC, Olsen MB, Kaasbøll OJ, Yang K, Fosshaug LE, Alfsnes K, Øgaard JDS, Rashidi A, Skulberg VM, Yang M, de Miranda Fonseca D, Sharma A, Aronsen JM, Schrumpf E, Ahmed MS, Dahl CP, Nyman TA, Ueland T, Melum E, Halvorsen BE, Bjørås M, Attramadal H, Sjaastad I, Aukrust P and Yndestad A. Absence of NLRP3 Inflammasome in Hematopoietic Cells Reduces Adverse Remodeling After Experimental Myocardial Infarction. *JACC Basic Transl Sci*. 2020;5:1210-1224.

29. Lim RM, Lu A, Chuang BM, Anaraki C, Chu B, Halbrook CJ and Edinger AL. CARMIL1-AA selectively inhibits macropinocytosis while sparing autophagy. *Mol Biol Cell*. 2025;36:ar4.

30. Koivusalo M, Welch C, Hayashi H, Scott CC, Kim M, Alexander T, Touret N, Hahn KM and Grinstein S. Amiloride inhibits macropinocytosis by lowering submembranous pH and preventing Rac1 and Cdc42 signaling. *J Cell Biol*. 2010;188:547-63.

31. Jia D, Chen S, Bai P, Luo C, Liu J, Sun A and Ge J. Cardiac Resident Macrophage-Derived Legumain Improves Cardiac Repair by Promoting Clearance and Degradation of Apoptotic Cardiomyocytes After Myocardial Infarction. *Circulation*. 2022;145:1542-1556.

32. Gong S, Zhai M, Shi J, Yu G, Lei Z, Shi Y, Zeng Y, Ju P, Yang N, Zhang Z, Zhang D, Zhuang J, Yu Q, Zhang X, Jian W, Wang W and Peng W. TREM2 macrophage promotes cardiac repair in myocardial infarction by reprogramming metabolism via SLC25A53. *Cell Death Differ*. 2024;31:239-253.

33. Jaitin DA, Adlung L, Thaiss CA, Weiner A, Li B, Descamps H, Lundgren P, Bleriot C, Liu Z, Deczkowska A, Keren-Shaul H, David E, Zmora N, Eldar SM, Lubezky N, Shibolet O, Hill DA, Lazar MA, Colonna M, Ginhoux F, Shapiro H, Elinav E and Amit I. Lipid-Associated Macrophages Control Metabolic Homeostasis in a Trem2-Dependent Manner. *Cell*. 2019;178:686-698.e14.

34. Ni B, Huang G, Yang R, Wang Z, Song H, Li K, Zhang Y, Wu K, Shi G, Wang X, Shen J and Liu Y. The short isoform of MS4A7 is a novel player in glioblastoma microenvironment, M2 macrophage polarization, and tumor progression. *Journal of Neuroinflammation*. 2023;20:80.

35. Zhao Q, Sheng MF, Wang YY, Wang XY, Liu WY, Zhang YY, Ke TY, Chen S, Pang GZ, Yong L, Ding Z, Shen YJ, Shen YX and Shao W. LncRNA Gm26917 regulates inflammatory response in macrophages by enhancing Annexin A1 ubiquitination in LPS-induced acute liver injury. *Front Pharmacol*. 2022;13:975250.

36. Chen M, Liang J, Ji H, Yang Z, Altilia S, Hu B, Schronce A, McDermott MSJ, Schools GP, Lim C-u, Oliver D, Shtutman MS, Lu T, Stark GR, Porter DC, Broude EV and Roninson IB. CDK8/19 Mediator kinases potentiate induction of transcription by NFκB. *Proceedings of the National Academy of Sciences*. 2017;114:10208-10213.

37. Junho CVC, Caio-Silva W, Trentin-Sonoda M and Carneiro-Ramos MS. An Overview of the Role of Calcium/Calmodulin-Dependent Protein Kinase in Cardiorenal Syndrome. *Front Physiol*. 2020;11:735.

38. Jung SH, Hwang BH, Shin S, Park EH, Park SH, Kim CW, Kim E, Choo E, Choi IJ, Swirski FK, Chang K and Chung YJ. Spatiotemporal dynamics of macrophage heterogeneity and a potential function of Trem2(hi) macrophages in infarcted hearts. *Nat Commun*. 2022;13:4580.

39. Wang PL, Yim AKY, Kim K-W, Avey D, Czepielewski RS, Colonna M, Milbrandt J and Randolph GJ. Peripheral nerve resident macrophages share tissue-specific programming and features of activated microglia. *Nature Communications*. 2020;11:2552.

40. Kumamoto Y, Camporez Joao Paulo G, Jurczak Michael J, Shanabrough M, Horvath T, Shulman GI and Iwasaki A. CD301b+ Mononuclear Phagocytes Maintain Positive Energy Balance through Secretion of Resistin-like Molecule Alpha. *Immunity*. 2016;45:583-596.

41. Calcagno DM, Ng RP, Toomu A, Zhang C, Huang K, Aguirre AD, Weissleder R, Daniels LB, Fu Z and King KR. The myeloid type I interferon response to myocardial infarction begins in bone marrow and is regulated by Nrf2-activated macrophages. *Science Immunology*. 2020;5:eaaz1974.

42. Blasius AL and Beutler B. Intracellular Toll-like Receptors. *Immunity*. 2010;32:305-315.

43. Coller SP and Paulnock DM. Signaling pathways initiated in macrophages after engagement of type A scavenger receptors. *Journal of Leukocyte Biology*. 2001;70:142-148.

44. Paulnock DM, Demick KP and Coller SP. Analysis of interferon-γ-dependent and -independent pathways of macrophage activation. *Journal of Leukocyte Biology*. 2000;67:677-682.

45. Masereel B, Pochet L and Laeckmann D. An overview of inhibitors of Na+/H+ exchanger. *European Journal of Medicinal Chemistry*. 2003;38:547-554.

46. Dai J and Sheetz MP. Regulation of endocytosis, exocytosis, and shape by membrane tension. *Cold Spring Harb Symp Quant Biol*. 1995;60:567-71.

47. Boulant S, Kural C, Zeeh JC, Ubelmann F and Kirchhausen T. Actin dynamics counteract membrane tension during clathrin-mediated endocytosis. *Nat Cell Biol*. 2011;13:1124-31.

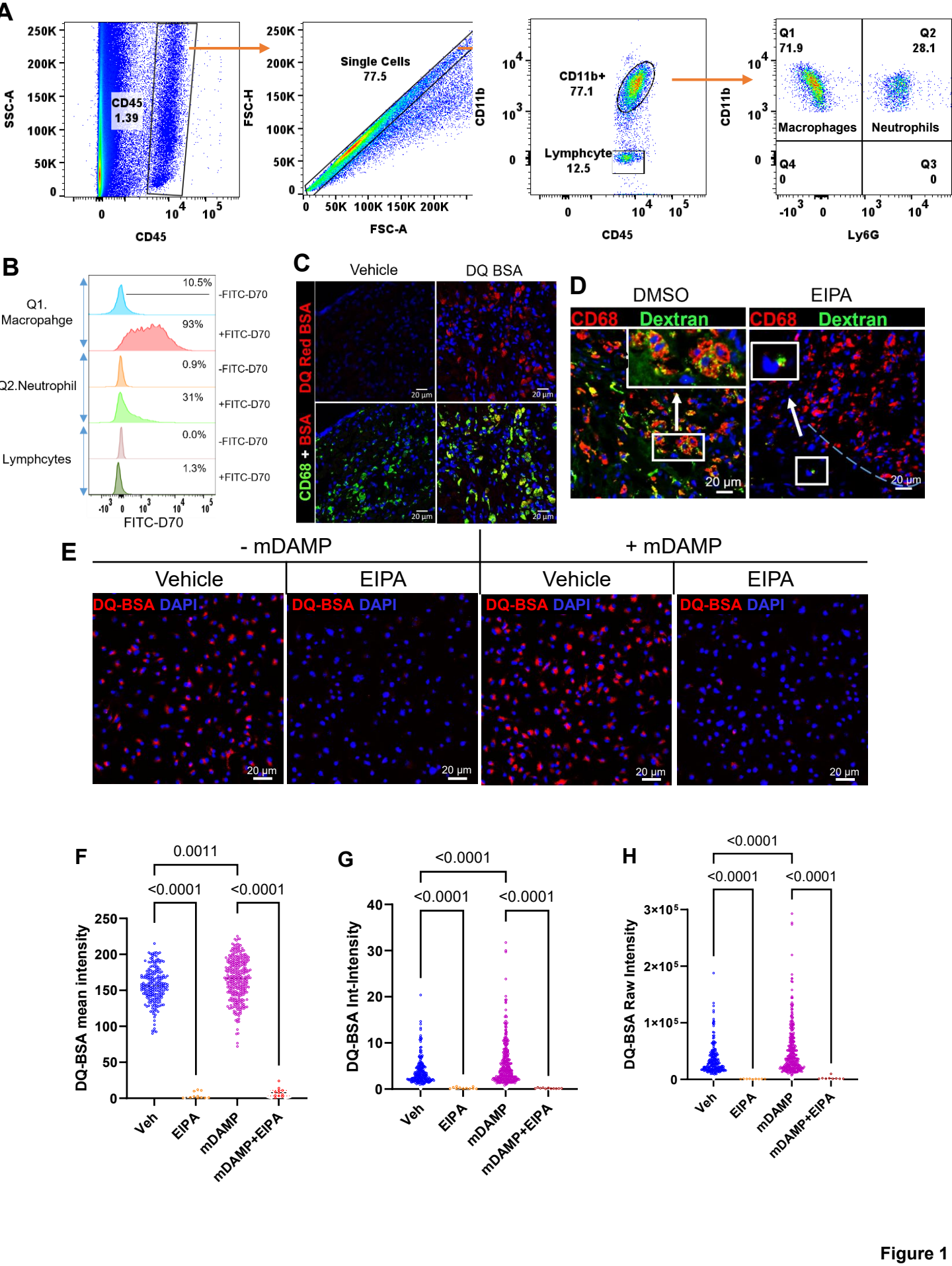
A
SSC-A
CD45
CD45
1.39
FSC-H
FSC-A
Single Cells
77.5
CD11b
CD45
CD11b+
77.1
Lymphcyte
12.5
CD11b
Ly6G
Q1
71.9
Q2
28.1
Macrophages
Neutrophils
Q4
0
Q3
0
B
Q1.
Macropahge
Q2.Neutrophil
Lymphcytes
10.5%
93%
0.9%
31%
0.0%
1.3%
-FITC-D70
+FITC-D70
FITC-D70
C
Vehicle
DQ BSA
DQ Red BSA
CD68 + BSA
20 µm
D
DMSO
EIPA
CD68
Dextran
20 µm
E
- mDAMP
+ mDAMP
Vehicle
EIPA
Vehicle
EIPA
DQ-BSA DAPI
20 µm
F
0.0011
<0.0001
<0.0001
DQ-BSA mean intensity
Veh
EIPA
mDAMP
mDAMP+EIPA
G
<0.0001
<0.0001
<0.0001
DQ-BSA Int-Intensity
H
<0.0001
<0.0001
<0.0001
DQ-BSA Raw Intensity

Figure 1

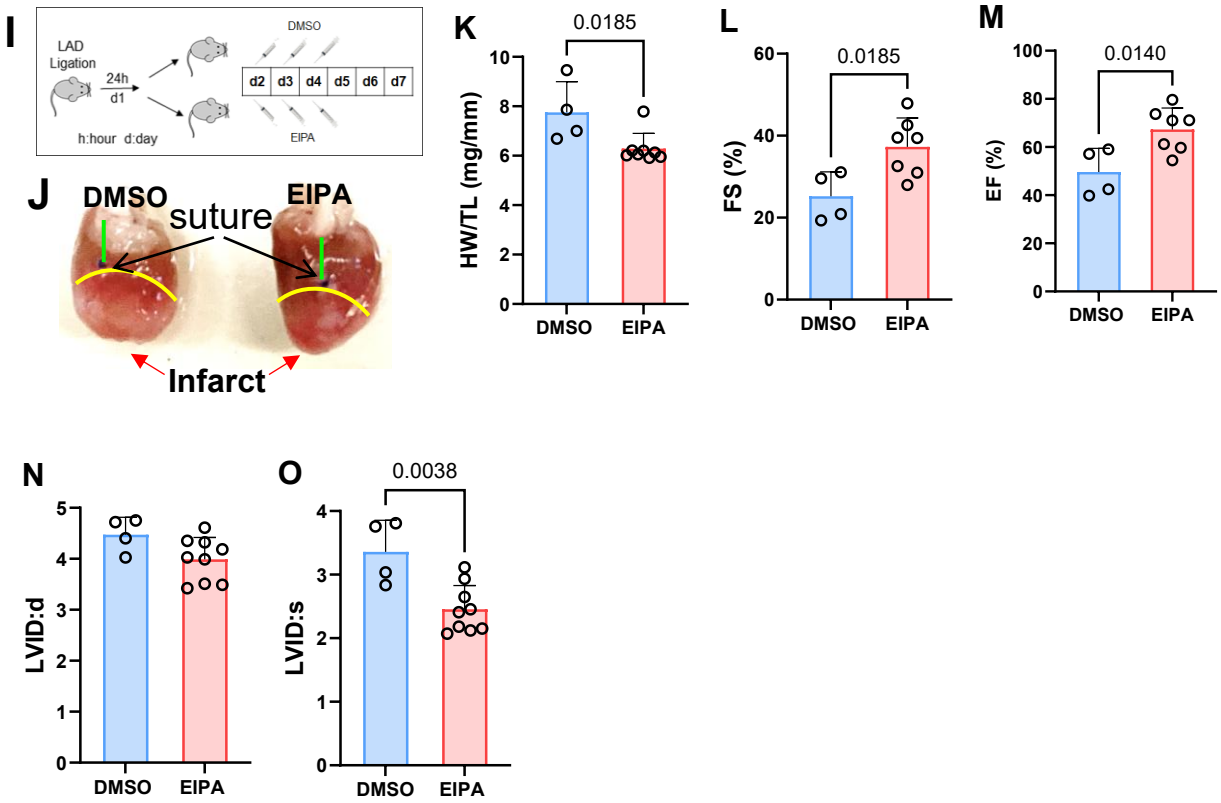

Figure 1. Inhibiting macropinocytosis in MI macrophages protects the heart from ischemic injury. Myocardial infarction was generated by LAD ligation for downstream analysis. **A.** Single cell suspension generated from the infarct tissue was incubated with FITC-Dextran 70 (D70) for 40 minutes, followed by labeling with CD45, CD11b, and Ly6G. Macrophages ($CD45^+CD11b^+Ly6G^-$), neutrophils ($CD45^+CD11b^+Ly6G^+$), and lymphocytes ($CD45^+CD11b^-Ly6G^-$) were gated. **B.** Percentages of cells uptaking the macropinocytosis reporter beads FITC-D70 demonstrate macrophages as the main cell type from the infarct with macropinocytosis. **C.** DQ-BSA, was diffused into the MI tissue. Tissue sections prepared were labeled with macrophage marker CD68. DQ-BSA signal (red) coincided with $CD68^+$ macrophages only. **D.** FITC-D70 was infused into the MI tissue in mice treated with DMSO or EIPA (12.5 mg/kg). Tissue sections were stained with CD68. Only $CD68^+$ macrophages engulfed the D70 and EIPA blocked the uptake of D70 by macrophages. **E.** BMDMs were incubated with DQ-BSA and stimulated w/wo mDAMP in the absence or presence of 10 μM EIPA. Images acquired to demonstrate the DQ-BSA signal in cells by confocal microscopy. **F,G,H.** The mean intensity, integrated intensity, and raw intensity of DQ-BSA were quantified using imageJ. Uptake of DQ-BSA was severely inhibited by EIPA treatment, consistent with the potent inhibitory effect of macropinocytosis. **I.** EIPA treatment scheme for MI mice. **J.** EIPA alleviated ischemic injury, demonstrating preserved conical apex morphology. EIPA treatment diminished ischemia-induced remodeling indicated by lower HW/TL (**K**), improved FS (**L**) and EF (**M**), and decreased end-systolic dimensions (**P**). Two-way ANOVA (F,G,H). Student's t-test (K to O).

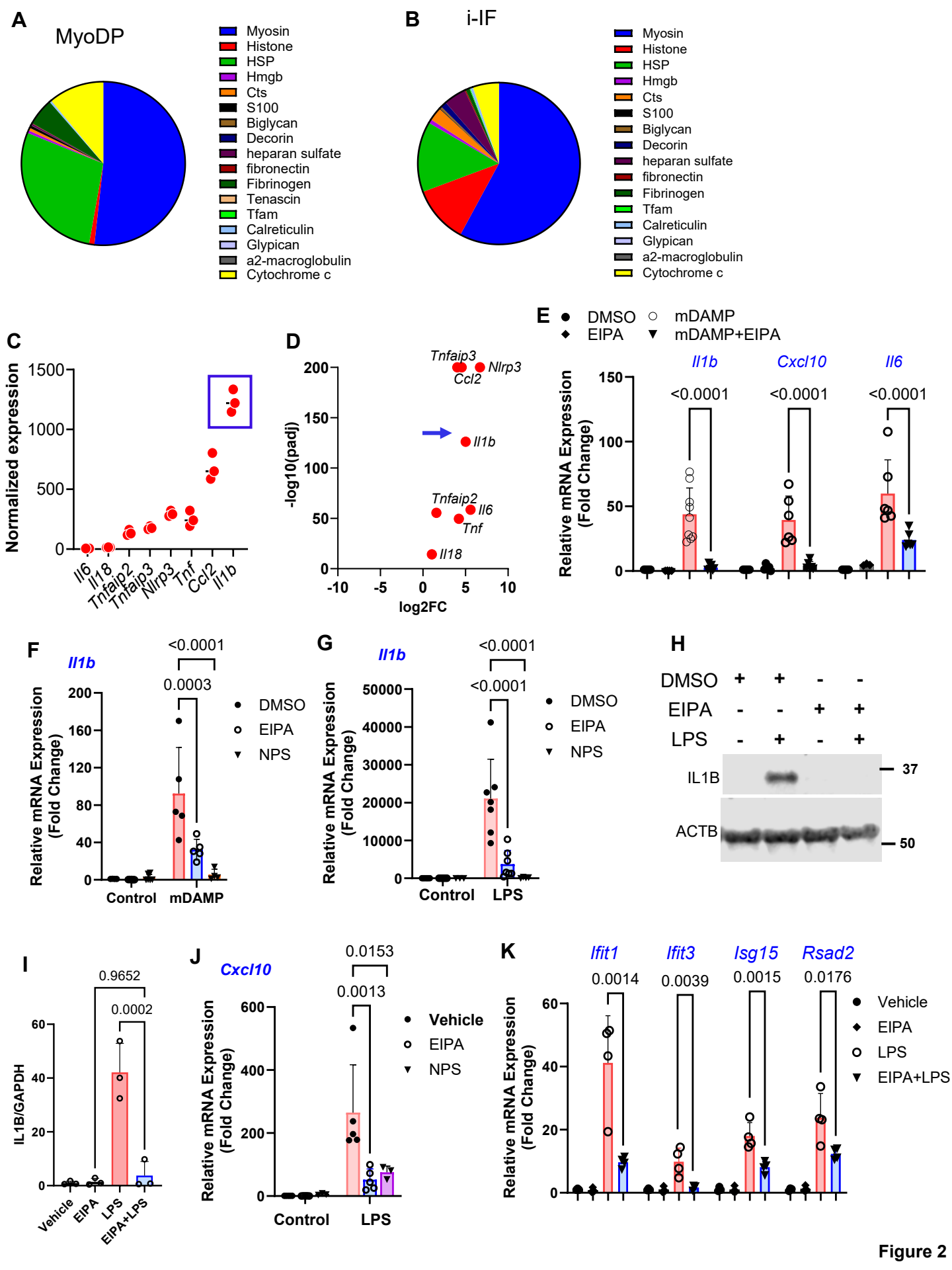
A
MyoDP
Myosin
Histone
HSP
Hmgb
Cts
S100
Biglycan
Decorin
heparan sulfate
fibronectin
Fibrinogen
Tenascin
Tfam
Calreticulin
Glypican
a2-macroglobulin
Cytochrome c
B
i-IF
Myosin
Histone
HSP
Hmgb
Cts
S100
Biglycan
Decorin
heparan sulfate
fibronectin
Fibrinogen
Tfam
Calreticulin
Glypican
a2-macroglobulin
Cytochrome c
C
Normalized expression
1500
1000
500
0
Il6
Il18
Tnfaip2
Tnfaip3
Nlrp3
Tnf
Ccl2
Il1b
D
-log10(padj)
200
150
100
50
0
Tnfaip3
Nlrp3
Ccl2
Il1b
Tnfaip2
Il6
Tnf
Il18
-10
-5
0
5
10
log2FC
E
DMSO
mDAMP
EIPA
mDAMP+EIPA
Il1b
Cxcl10
Il6
<0.0001
<0.0001
<0.0001
Relative mRNA Expression (Fold Change)
150
100
50
0
F
Il1b
<0.0001
0.0003
Relative mRNA Expression (Fold Change)
200
160
120
80
40
0
DMSO
EIPA
NPS
Control
mDAMP
G
Il1b
<0.0001
<0.0001
Relative mRNA Expression (Fold Change)
50000
40000
30000
20000
10000
0
DMSO
EIPA
NPS
Control
LPS
H
DMSO + + - -
EIPA - - + +
LPS - + - +
IL1B
ACTB
37
50
I
0.9652
0.0002
IL1B/GAPDH
60
40
20
0
Vehicle
EIPA
LPS
EIPA+LPS
J
Cxcl10
0.0153
0.0013
Relative mRNA Expression (Fold Change)
600
400
200
0
Vehicle
EIPA
NPS
Control
LPS
K
Ifit1
Ifit3
Isg15
Rsad2
0.0014
0.0039
0.0015
0.0176
Relative mRNA Expression (Fold Change)
60
40
20
0
Vehicle
EIPA
LPS
EIPA+LPS

Figure 2

Figure 2. Inhibiting macropinocytosis interferes with TLR4-mediated signaling. A. Proteomic analysis of DAMP composition of the extracellular fluid isolated from infarct tissue. **B.** Proteomic analysis of DAMP composition of mDAMP extracted from enriched mitochondria of the myocardium. **C.** MI macrophages were purified by FACS. Bulk RNAseq analysis demonstrates *Il1b* as the most prevalent inflammatory cytokine expressed in MI macrophages. **D.** Bone marrow monocytes and MI macrophages were purified by FACS. Bulk RNAseq Bulk RNAseq analysis revealed *Il1b* as one of the most significantly upregulated cytokines when compared to BM monocytes, the precursor cells. **E.** BMDMs were stimulated with mDAMP+/-EIPA (10 μM) for 4 h followed by RNA extraction. mDAMP-induced expressions of *Il1b*, *Cxcl*10, and *Il6* were suppressed by macropinocytosis inhibitor EIPA. **F.** Experiments performed as described in **E** with BMDMs treated with EIPA or NPS (3μM), a structurally different macropinocytosis inhibitor. NPS abolished mDMAP-induced *Il1b* expression. **G.** BMDMs were stimulated with LPS (10 ng/ml) for 4 h without or with EIPA or NPS. The Il1b expression was markedly inhibited by EIPA and NPS. **H and I.** EIPA completely blocked IL1B protein expression-induced by LPA. **J and K.** EIPA significantly reduced LPS-induced expression of ISGs, including *Cxcl10*, *Ifit1*, *Ifit3*, *Isg15*, and *Rsad2*. Two-way ANOVA (E, F G, I). Student's t-test (J, K)

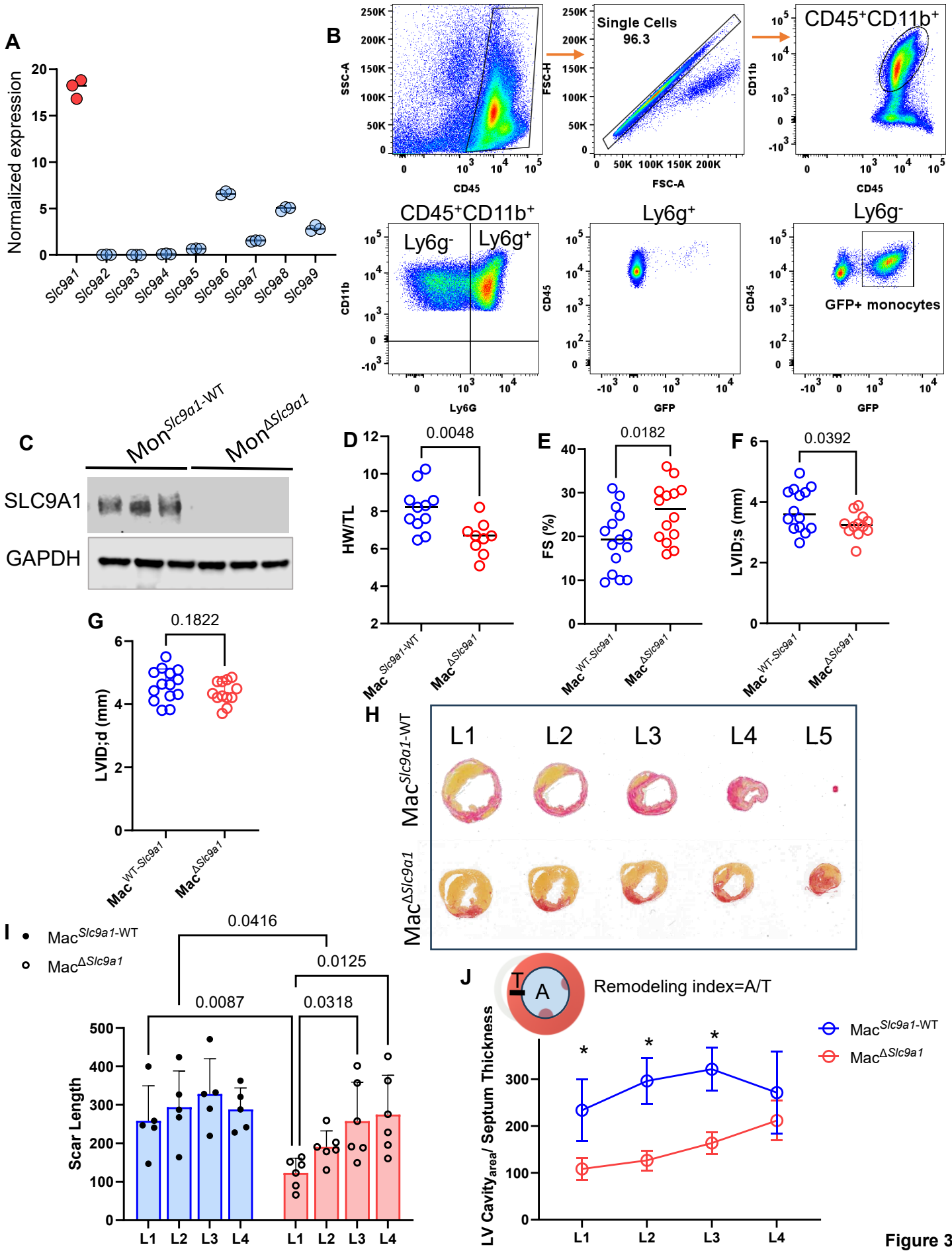
A
Normalized expression
Slc9a1
Slc9a2
Slc9a3
Slc9a4
Slc9a5
Slc9a6
Slc9a7
Slc9a8
Slc9a9
B
SSC-A
CD45
FSC-H
FSC-A
Single Cells
96.3
CD45+CD11b+
CD11b
Ly6g-
Ly6g+
Ly6G
GFP
GFP+ monocytes
C
Mon Slc9a1-WT
Mon ΔSlc9a1
SLC9A1
GAPDH
D
HW/TL
0.0048
E
FS (%)
0.0182
F
LVID;s (mm)
0.0392
G
LVID;d (mm)
0.1822
Mac WT-Slc9a1
Mac ΔSlc9a1
H
L1
L2
L3
L4
L5
Mac Slc9a1-WT
Mac ΔSlc9a1
I
Mac Slc9a1-WT
Mac ΔSlc9a1
Scar Length
0.0416
0.0125
0.0087
0.0318
J
T
A
Remodeling index=A/T
LV Cavity area/ Septum Thickness
Mac Slc9a1-WT
Mac ΔSlc9a1

Figure 3

Figure 3. Macrophage-specific deletion of *Slc9a1* protected the heart from ischemic injury. A. Bone marrow monocytes were purified by FACS. Normalized expression levels by bulk RNA-seq analysis demonstrated that *Slc9a1* was the main isoform of the SLC9A1 family. **B.** Gating strategy to isolate bone marrow monocytes with endogenous GFP or using the gating strategy $CD45^{+}CD11b^{+}Ly6G^{-}Ly6c^{hi}CCR2^{+}$. The *Slc9a1*$^{f/f}$;CCR2-Cre-GFP mice and control littermates (*Slc9a1*$^{f/f}$ or CCR2-Cre-GFP) were given tamoxifen (TMX) injection via i.p. at 75mg/kg/day for three days. After the injection, these mouse cohorts were annotated as Monocyte(Mon)$^{\Delta Slc9a1}$ and Mon$^{Slc9a1\text{-WT}}$. **C.** Protein samples of BM monocytes purified from Mon$^{\Delta Slc9a1}$ and Mon$^{Slc9a1\text{-WT}}$ mice were subjected to SDS-PAGE. The lack of SLC9A1 in samples from Mon$^{\Delta Slc9a1}$ confirmed the conditional deletion. **D,E,F.** Myocardial infarction was generated by LAD ligation in Mon$^{\Delta Slc9a1}$ and Mon$^{Slc9a1\text{-WT}}$ mice. Remodeling parameters were measured 7 dpi. Specifically deleting *Slc9a1* from MDM, annotated as Macrophage(Mac)$^{\Delta Slc9a1}$, decreased HW/TL ratio (**D**), improved cardiac function (FS, **E**), and decreased end-systolic dimension (**F**). **G.** Representative cross-sections from the base to the apex depict LV morphology and scar sizes. **H.** Quantification of scar length from sections at different levels as indicated on G. **I.** Plot of remodeling index (RI), calculated by dividing LV diameter with the septum thickness (illustrated by the diagram), in Mac$^{\Delta Slc9a1}$ and Mac$^{Slc9a1\text{-WT}}$ mice. Student's t-test.

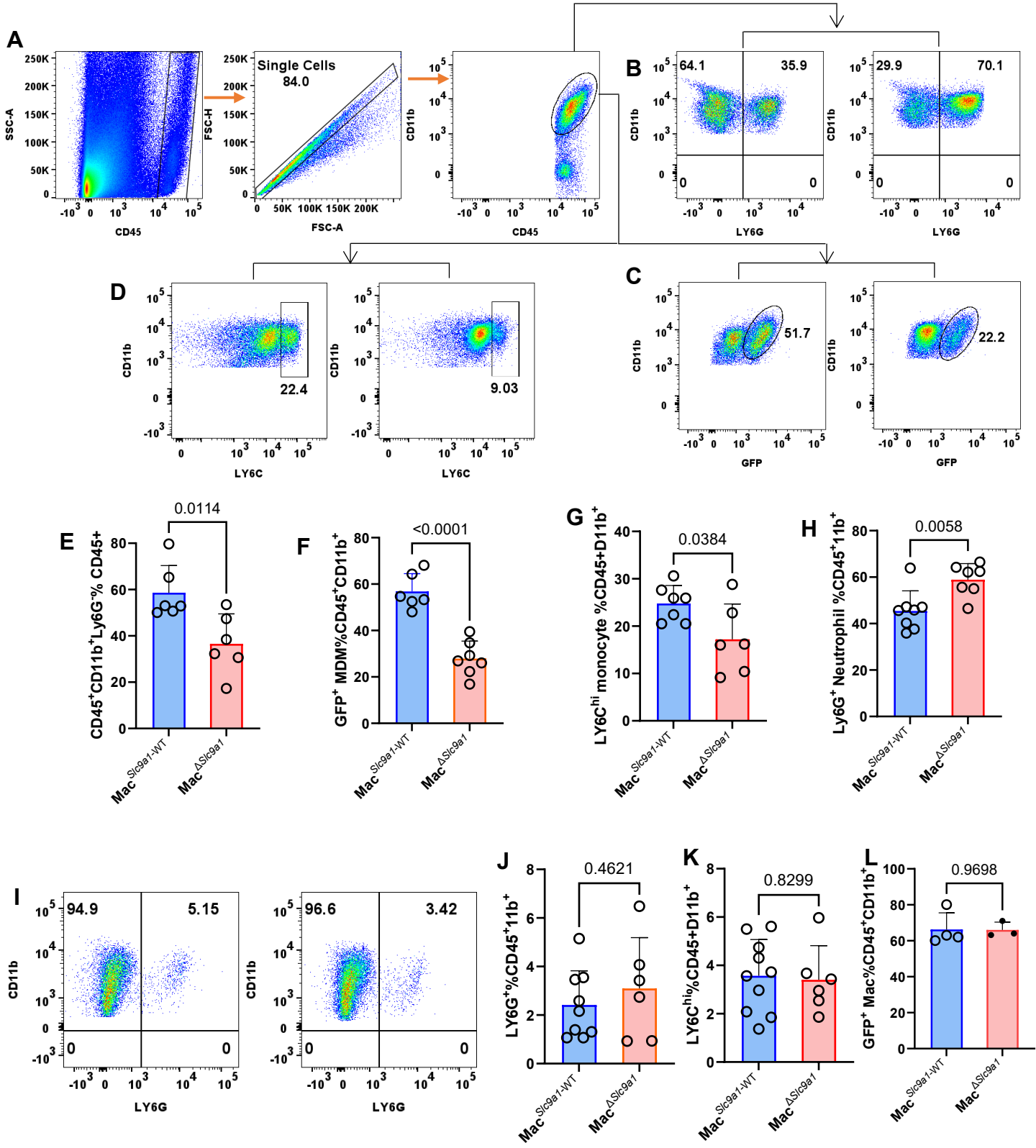
A
SSC-A
CD45
FSC-H
Single Cells
84.0
FSC-A
CD11b
B
64.1
35.9
29.9
70.1
LY6G
C
51.7
22.2
GFP
D
22.4
9.03
LY6C
E
0.0114
CD45+CD11b+Ly6G-% CD45+
Mac Slc9a1-WT
Mac ΔSlc9a1
F
<0.0001
GFP+ MDM%CD45+CD11b+
G
0.0384
LY6Chi monocyte %CD45+D11b+
H
0.0058
Ly6G+ Neutrophil %CD45+11b+
I
94.9
5.15
96.6
3.42
J
0.4621
LY6G+%CD45+11b+
K
0.8299
LY6Chi%CD45+D11b+
L
0.9698
GFP+ Mac%CD45+CD11b+

Figure 4

Figure 4. Cardiac immune phenotyping of the Mac$^{\Delta Slc9a1}$ and Mac$^{Slc9a1\text{-}WT}$ mice. after myocardial infarction. A. Single cell suspension from the MI tissue was gated for the myeloid population ($CD45^+CD11b^+$). **B.** Total macrophage population ($CD45^+CD11b^+Ly6G^-$). **C.** GFP^+MDM: $CD45^+CD11b^+Ly6G^-GFP^+$ **D.** Recently recruited monocytes: $CD45^+CD11b^+Ly6G^-y6C^{hi}$. Neutrophils: $CD45^+CD11b^+Ly6G^+y6C^{int}GFP^-$. **E,F,G.** Quantification of the total macrophages (E), MDM (F), and newly-recruited monocytes (G) demonstrates that conditional deletion of *Slc9a1* reduced infiltration of monocytes and accumulation of macrophages 3dpi. **H.** Conditional deletion of *Slc9a1* increased neutrophil prevalence in the infarct tissue 3dpi. **I,J.** Neutrophils were efficiently removed at 7dpi in the infarct of both Mac$^{\Delta Slc9a1}$ and Mac$^{Slc9a1\text{-}WT}$ mice. K**,L.** No significant difference in monocyte total MDM in the MI of Mac$^{\Delta Slc9a1}$ and Mac$^{Slc9a1\text{-}WT}$ mice 7dpi. Student's t-test.

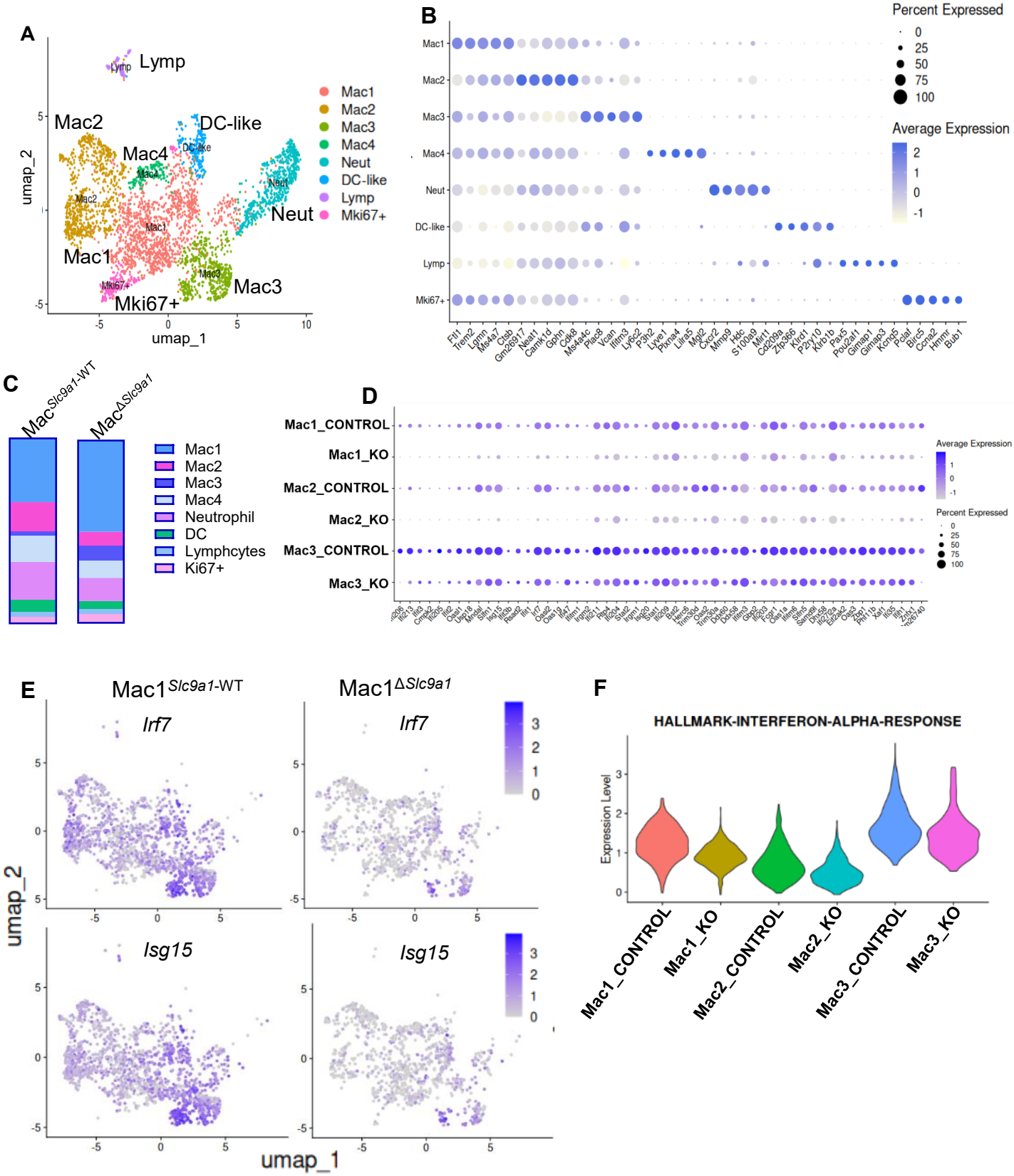
A
Lymp
Mac2
DC-like
Mac4
Neut
Mac1
Mac3
Mki67+
umap_1
umap_2
Mac1
Mac2
Mac3
Mac4
Neut
DC-like
Lymp
Mki67+
B
Percent Expressed
0
25
50
75
100
Average Expression
2
1
0
-1
Mac1
Mac2
Mac3
Mac4
Neut
DC-like
Lymp
Mki67+
Ftl1 Trem2 Lgmn Ms4a7 Ctsb Gm26917 Neat1 Camk1d Gpnh Cd48 Ms4a4c Plac8 Vcan Ifitm3 Ly6c2 P3h2 Lyve1 Pkma4 Lilra5 Mgl2 Cxcr2 Mmp9 Hdc S100a9 Mirt1 Cd209a Zfp366 Klrd1 P2ry10 Klrb1b Pax5 Pou2af1 Gimap1 Gimap3 Kcnq5 Pclaf Birc5 Ccna2 Hmmr Bub1
C
MacSlc9a1-WT
MacΔSlc9a1
Mac1
Mac2
Mac3
Mac4
Neutrophil
DC
Lymphcytes
Ki67+
D
Mac1_CONTROL
Mac1_KO
Mac2_CONTROL
Mac2_KO
Mac3_CONTROL
Mac3_KO
Average Expression
Percent Expressed
E
Mac1Slc9a1-WT
Mac1ΔSlc9a1
Irf7
Isg15
umap_1
umap_2
F
HALLMARK-INTERFERON-ALPHA-RESPONSE
Expression Level
Mac1_CONTROL
Mac1_KO
Mac2_CONTROL
Mac2_KO
Mac3_CONTROL
Mac3_KO

Figure 5

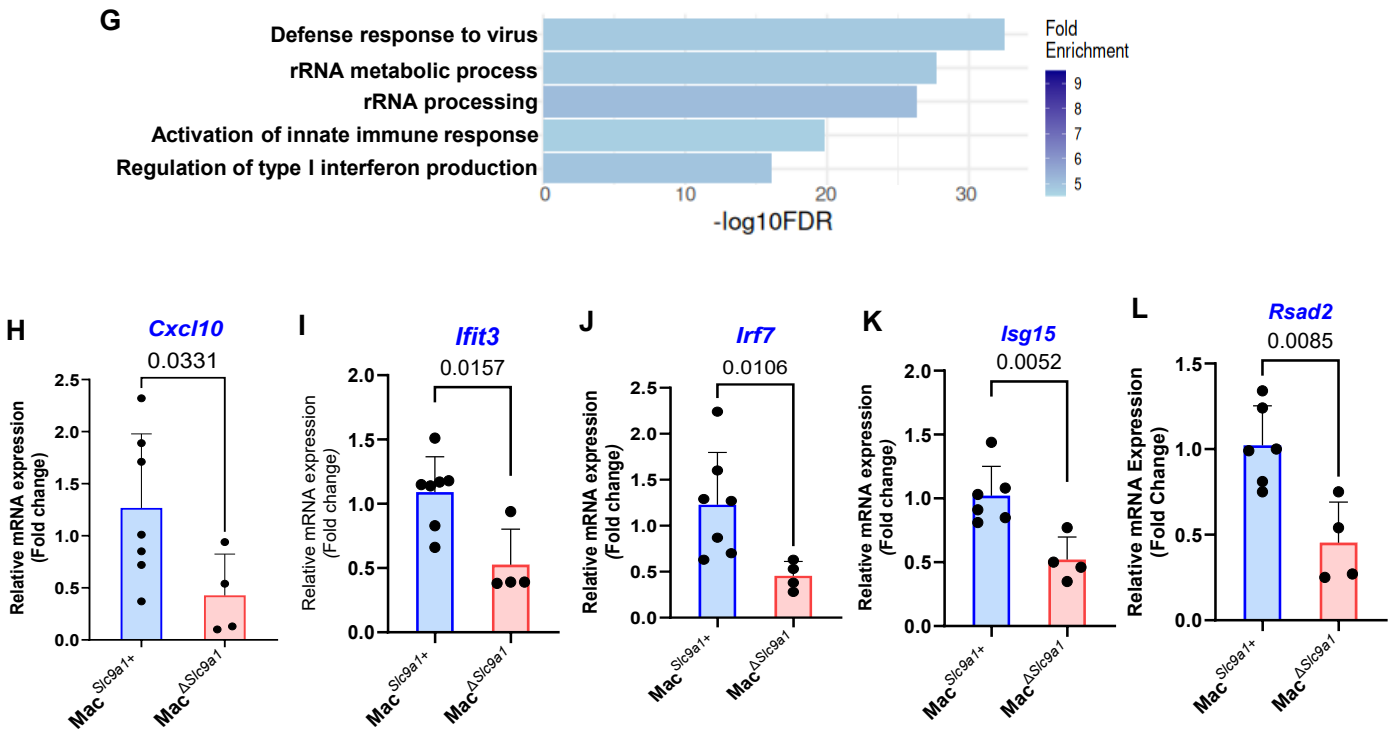

Figure 5. SLC9A1 promoted interferon stimulated genes response in acute ischemia in MDM. Myeloid cells from the infarct 4dpi. were first enriched using CD45+ antibody coupled with magnetic beads followed FACS to purify $CD45^{+}CD11b^{+}CD3^{-}$ cells. The cells were subjected to 10x Genomic plateform for scRNA-seq analysis. **A,B.** The UMAP demonstrates 8 clusters of cells (A), which were annotated based on marker genes depicted in B. **C.** The proportion of each cluster. **D.** Dot plots depict the average expression of 48 ISGs in macrophage (Mac) cluster 1, Mac 2, and Mac 3, which were down-regulated in Slc9a1-deficient cells. **E.** The expression level of *Ifr7* and *Isg15* on UMAP, which were decreased Mac1 from $Mac^{\Delta Slc9a1}$ MI. **F.** The violin plot depicts Hallmark Interferon Alpha response from Mac1, Mac2, and Mac3 from control and *Slc9a1* conditional knockout MI hearts. **G.** GO enrichment analysis demonstrates down-regulation of pathways in *Slc9a1*-deficient Mac1. **H,I,J,K,I.** Total RNA was purified from MI tissue 3dpi and the expressions of a group of ISGs, including *Cxcl10* (H), *Ifit3* (I), *Irf7* (J), *Isg15* (K), and *Rsad2* (L) were measured using RT-qPCR. Student's t-test.

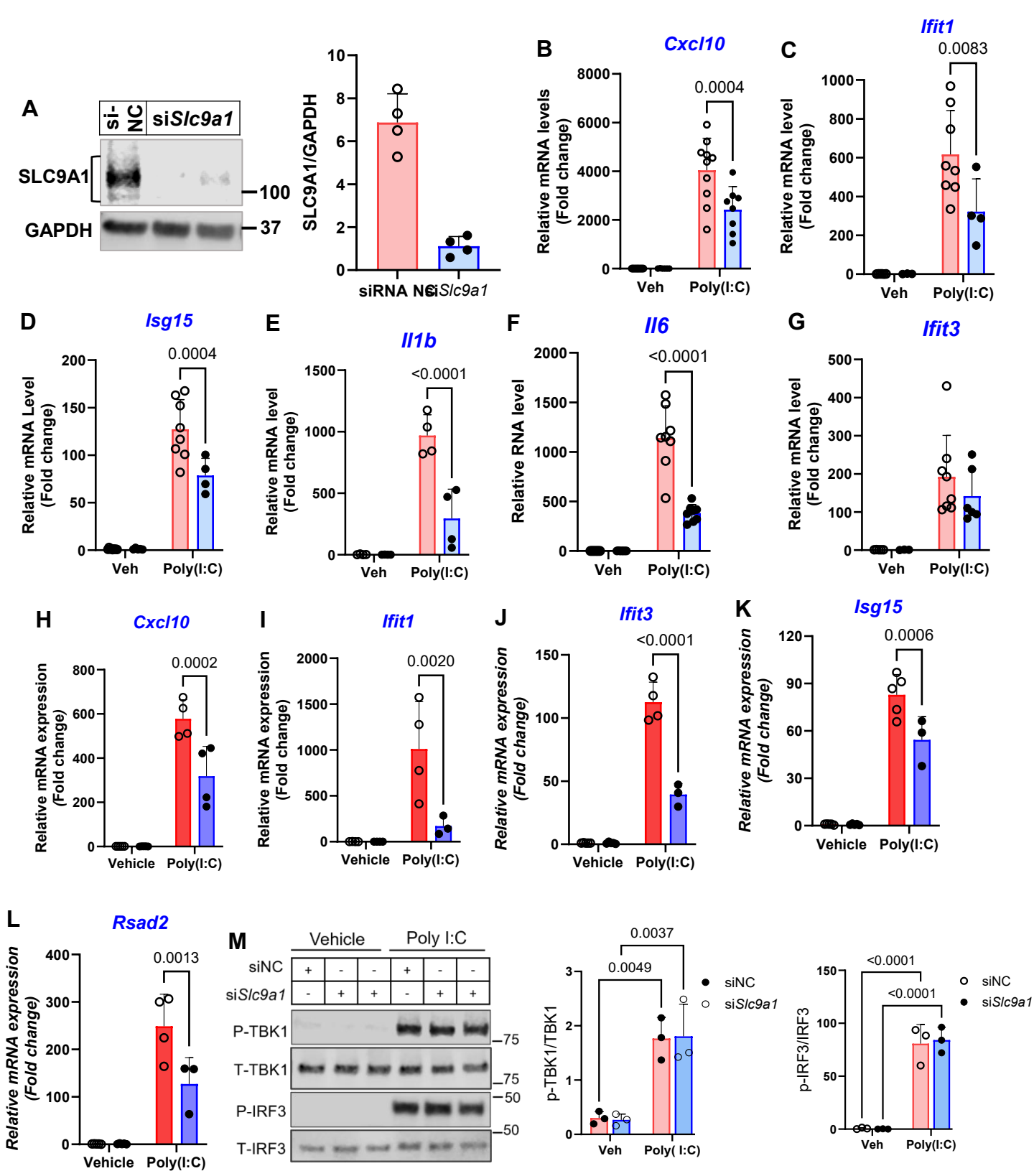
A
si-NC
siSlc9a1
SLC9A1
GAPDH
100
37
SLC9A1/GAPDH
siRNA NC
siSlc9a1
B
Cxcl10
Relative mRNA levels (Fold change)
0.0004
Veh
Poly(I:C)
C
Ifit1
0.0083
Relative mRNA level (Fold change)
D
Isg15
0.0004
Relative mRNA Level (Fold change)
E
Il1b
<0.0001
Relative mRNA level (Fold change)
F
Il6
<0.0001
Relative RNA level
G
Ifit3
Relative mRNA level (Fold change)
H
Cxcl10
0.0002
Relative mRNA expression (Fold change)
Vehicle
I
Ifit1
0.0020
J
Ifit3
<0.0001
K
Isg15
0.0006
L
Rsad2
0.0013
M
Vehicle
Poly I:C
siNC
siSlc9a1
P-TBK1
T-TBK1
P-IRF3
T-IRF3
75
50
0.0037
0.0049
p-TBK1/TBK1
p-IRF3/IRF3

Figure 6

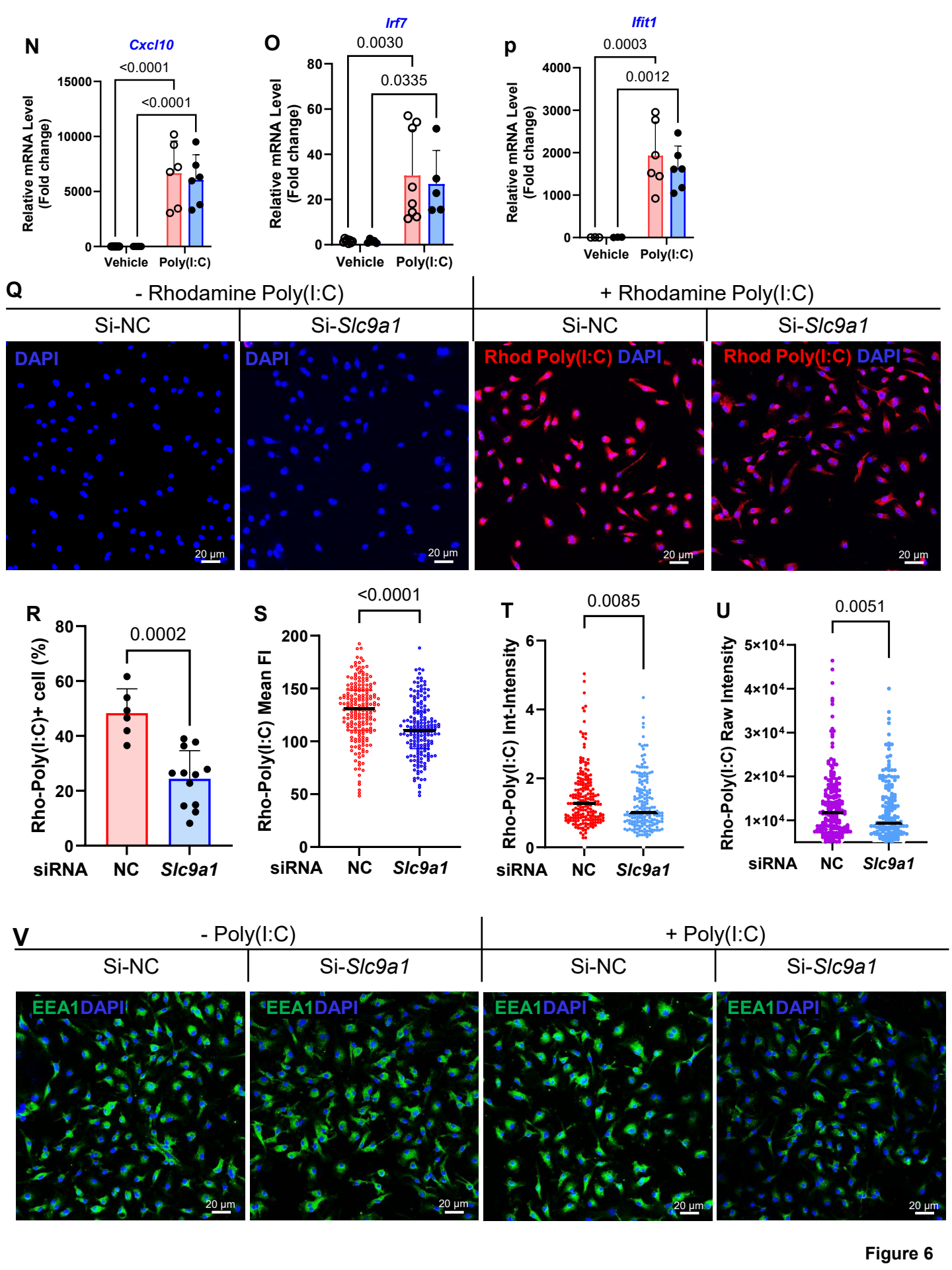
N
Cxcl10
<0.0001
<0.0001
Relative mRNA Level (Fold change)
15000
10000
5000
0
Vehicle
Poly(I:C)
O
Irf7
0.0030
0.0335
Relative mRNA Level (Fold change)
80
60
40
20
0
Vehicle
Poly(I:C)
p
Ifit1
0.0003
0.0012
Relative mRNA Level (Fold change)
4000
3000
2000
1000
0
Vehicle
Poly(I:C)
Q
- Rhodamine Poly(I:C)
+ Rhodamine Poly(I:C)
Si-NC
Si-Slc9a1
Si-NC
Si-Slc9a1
DAPI
DAPI
Rhod Poly(I:C) DAPI
Rhod Poly(I:C) DAPI
20 μm
20 μm
20 μm
20 μm
R
0.0002
Rho-Poly(I:C)+ cell (%)
80
60
40
20
0
siRNA
NC
Slc9a1
S
<0.0001
Rho-Poly(I:C) Mean FI
200
150
100
50
0
siRNA
NC
Slc9a1
T
0.0085
Rho-Poly(I:C) Int-Intensity
6
4
2
0
siRNA
NC
Slc9a1
U
0.0051
Rho-Poly(I:C) Raw Intensity
5×10⁴
4×10⁴
3×10⁴
2×10⁴
1×10⁴
siRNA
NC
Slc9a1
V
- Poly(I:C)
+ Poly(I:C)
Si-NC
Si-Slc9a1
Si-NC
Si-Slc9a1
EEA1DAPI
EEA1DAPI
EEA1DAPI
EEA1DAPI
20 μm
20 μm
20 μm
20 μm

Figure 6

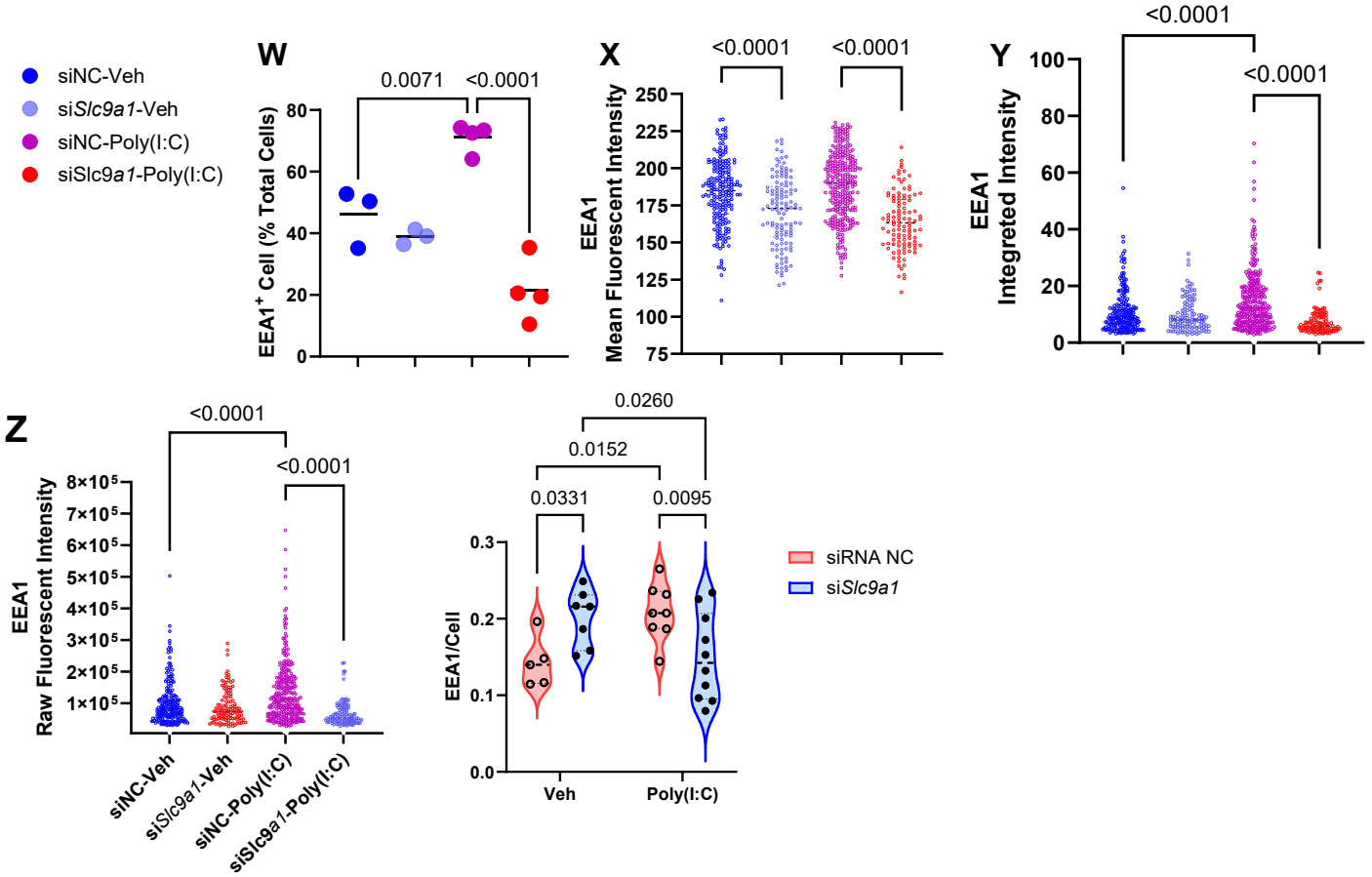

Figure 6. SLC9A1 promoted TLR3 signaling by increasing the endocytosis of its ligand Poly(I:C). A. BMDMs were treated with siNC and si*Slc9a1* for 24 h. SLC9A1 protein was quantified after immunoblot analysis four days after the siRNA treatment. **B to F.** Inhibiting SLC9A1 mitigated Poly(I:C)-induced ISG expression (*Cxcl10* (B), *Ifit1* (C), *Isg15* (D)) and inflammatory cytokines (*Il1b* (E) and *Il6* (F)). **G.** Knocking-down *Slc9a1* did not significantly affect *Ifit3.* **H to L.** Control (Mon$^{Slc9a1\text{-WT}}$) and mice with monocyte-specific *Slc9a1* deletion (Mon$^{\Delta Slc9a1}$) were generated with TMX injection. ISG expressions were quantified by RT-qPCR, demonstrating *Slc9a1* deletion suppressed Poly(I:C)-induced expression of *Cxcl10* (H), *Ifit1* (I), *Ifit3* (J), *Isg15* (K), and *Rsad2* (L). **M to P,** BMDM obtained as described in A were transfected with Poly(I:C) at 500 ng/ml. Protein samples and RNAs were purified 4 h after the transfection. The phosphorylated TBK1 and IRF3 were along with total isoforms are demonstrated and the quantified TBK1 and IRF3 activation is depicted in M. The ISG expression, including *Cxcl10* (N), *Irf7* (O), *Ifit1* (P), were measured by RT-qPCR. **Q.** BMDM obtained as in A were treated with vehicle or Rhodamine-Poly(I;C) for 1 h. Images were obtained using confocal microscopy after the treatment. **R to U.** Rhodamine-Poly(I:C) uptake was quantified using ImageJ. Quantification from 2 to 4 fields of individual experiment were included in the summary graph. *Slc9a1* knocking-down decreased the proportion of cells with detectable Poly(I:C) (R), reduced the mean, integrated, and raw Poly(I:C) intensity (**S to U). V.** BMDM obtained as described in A were stimulated with Poly(I:C) at 5 μM for 4 h. The early endosomes were labeled with the specific marker EEA1. Images were acquired using confocal-imaging. **W to Z.** The early endosomes were quantified using ImageJ. Knocking-down *Slc9a1* decreased proportion of cells with detectable early endosomes after poly(I:C) stimulation (W), decreased the mean, integrated, and raw intensity of EEA1-labeled early endosomes (Y,Y,Z). Student t-test (R,S,T,U). Two-way ANOVA for the rest.

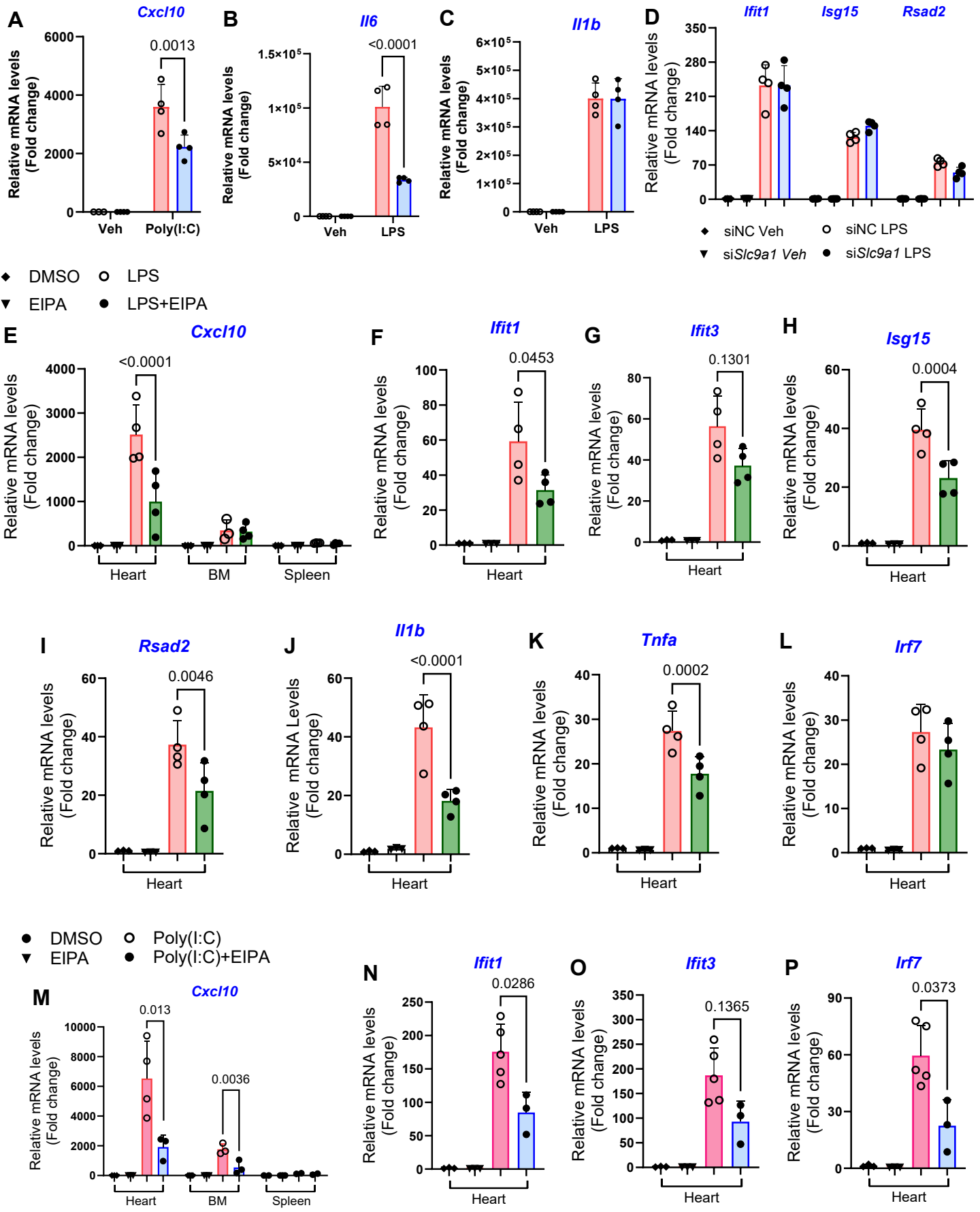
A
Cxcl10
0.0013
Relative mRNA levels (Fold change)
Veh
Poly(I:C)
B
Il6
<0.0001
Relative mRNA levels (Fold change)
Veh
LPS
C
Il1b
Relative mRNA levels (Fold change)
Veh
LPS
D
Ifit1
Isg15
Rsad2
Relative mRNA levels (Fold change)
siNC Veh
siNC LPS
siSlc9a1 Veh
siSlc9a1 LPS
DMSO
LPS
EIPA
LPS+EIPA
E
Cxcl10
<0.0001
Relative mRNA levels (Fold change)
Heart
BM
Spleen
F
Ifit1
0.0453
Relative mRNA levels (Fold change)
Heart
G
Ifit3
0.1301
Relative mRNA levels (Fold change)
Heart
H
Isg15
0.0004
Relative mRNA levels (Fold change)
Heart
I
Rsad2
0.0046
Relative mRNA levels (Fold change)
Heart
J
Il1b
<0.0001
Relative mRNA Levels (Fold change)
Heart
K
Tnfa
0.0002
Relative mRNA levels (Fold change)
Heart
L
Irf7
Relative mRNA levels (Fold change)
Heart
DMSO
Poly(I:C)
EIPA
Poly(I:C)+EIPA
M
Cxcl10
0.013
0.0036
Relative mRNA levels (Fold change)
Heart
BM
Spleen
N
Ifit1
0.0286
Relative mRNA levels (Fold change)
Heart
O
Ifit3
0.1365
Relative mRNA levels (Fold change)
Heart
P
Irf7
0.0373
Relative mRNA levels (Fold change)
Heart

Figure 7

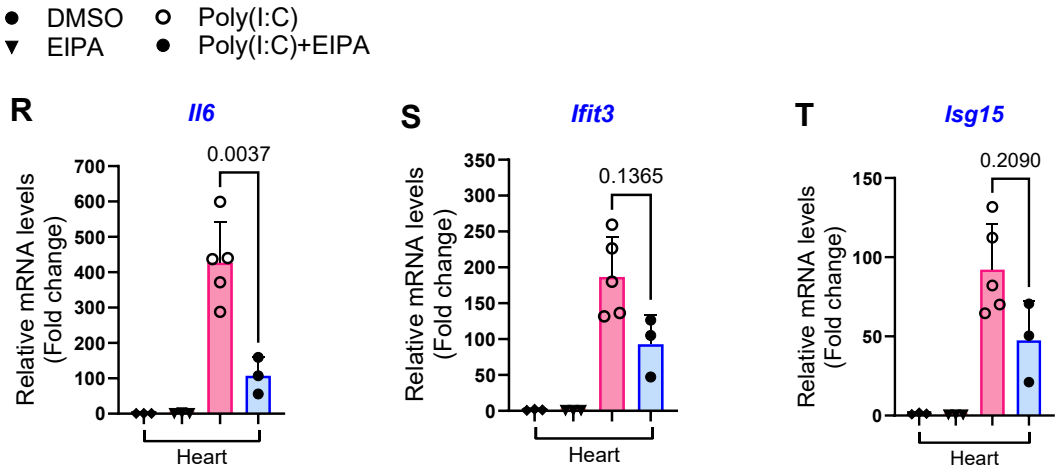

Figure 7. Pharmacological inhibition of SLC9A inhibits cardiac inflammatory responses to systemically administered LPS and Poly(I:C). A to D. BMDMs were treated with siNC or si*Slc9a1*. These cells were then stimulated with LPS at 10 ng/ml for 4 h. **A and B**. Knocking down *Slc9a1* significantly inhibited *Cxcl10* and *Il6* expression. **C and D.** Limited impact of reducing SLC9A1 on *Il1b*, *Ifit1*, *Isg15*, and *Rsad2 expression-induced by LPS*. **E to T.** C57BLK6/J mice were treated with daily injection of EIPA for two days before IPS or Poly(I:C) challenge via i.p. injection. Four hours after the injection, tissues (heart, spleen, and BM) were collected and flash-frozen with liquid nitrogen for downstream analysis. Total RNA was extracted for RT-qPCR. **E to L.** Vehicle and LPS-challenged mouse cohort. The heart had the most robust response to LPS (A). EIPA treatment significantly dampened the inflammatory response by decreasing the expression of *Cxcl10* (A), *Ifit1* (B), *Ifit3* (C), *Isg15* (D), *Rsad2* (E), *Il1b* (F), *Tnfa* (G), while had no effect on *Irf7* (H). **M to T.** Poly(I:C) challenged mouse cohorts. The heart responded to Poly(I:C) the strongest among the three organs (heart, spleen, and BM) (I). EIPA treatment significantly inhibited cardiac response to Poly(I:C) by suppressing the expression of *Cxcl10* (I), *Ifit1* (J), *Ifit3* (K), *Irf7* (L), *Isg15* (M), *Rsad2* (N), and *Il6* (O). Two-way ANOVA.

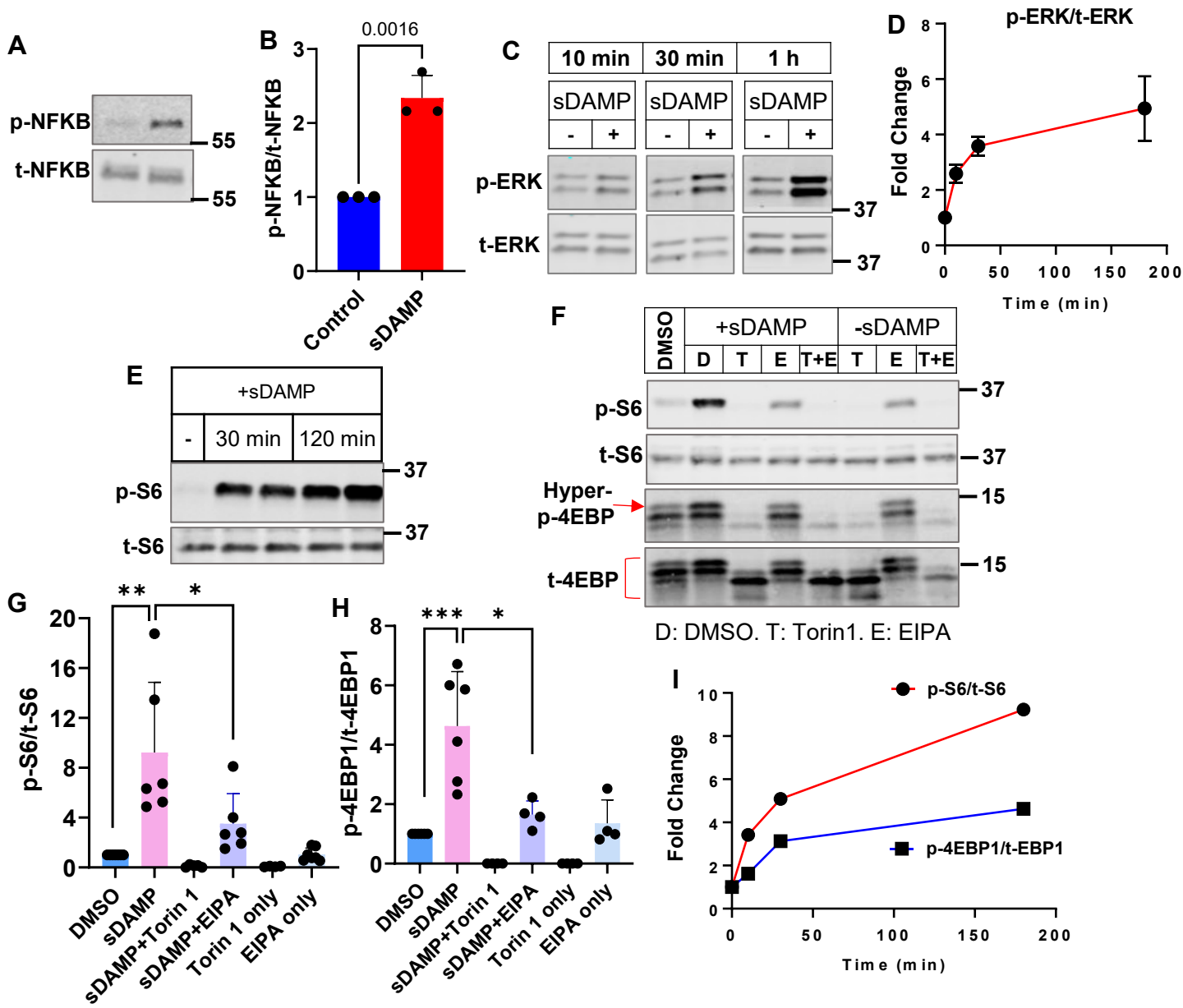

Supplemental. Figure 1. mDAMP simulates TLR agonist by triggering acute activation of NFKB, ERK, and mTORC1. BMDMs were treated with mDAMP. Protein samples extracted after the treatment were subjected to SDS-PAGE and immunoblot analysis. **A and B.** The phosphorylation/activation of NFKB after 4 h treatment of mDAMP. The bar graph depicts summarized results from different experiments. **C and D.** ERK activation by mDAMP. The time course of ERK activation is summarized in D. **E and F.** Phosphorylation of S6 and hyper-phosphorylation of 4EBP1 after 4 h mDAMP stimulation. **G and H.** Summarized results from individual experiments as performed in E and F. **I.** The time course of S6 phosphorylation. Student t-test (B). Two-way ANOVA (G, H).

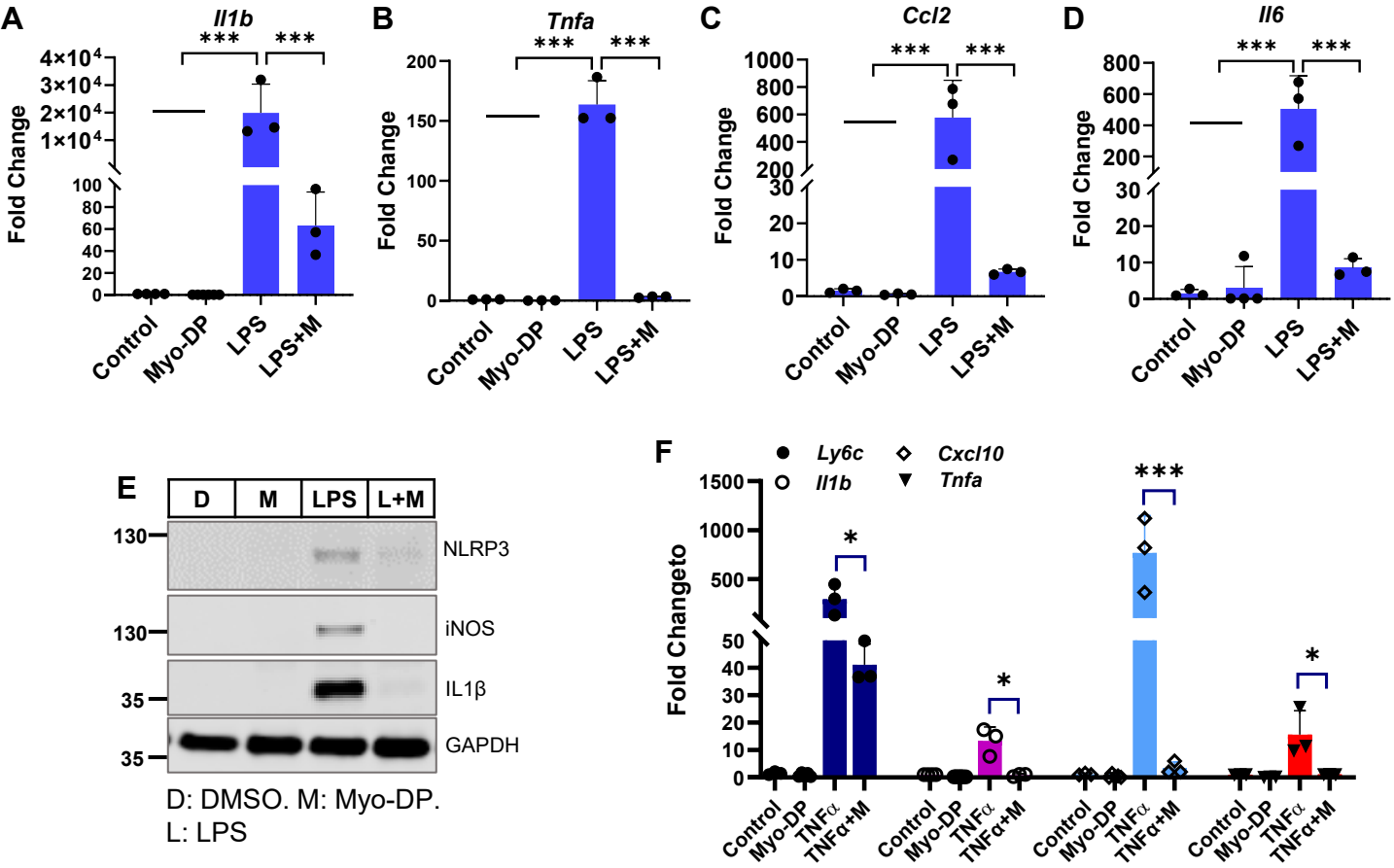

Supplemental. Figure 2. The precursor (myo-DP) of mDAMP did not induce inflammatory cytokine expression. Mitochondria were enriched from myocardium obtained from mice at baseline. The preparation is named myocardium-derived preparation (Myo-DP). Myo-DP was the precursor material of the mDAMP. BMDMs were treated with Myo-DP. LPS was used as a positive control. Protein samples extracted after the treatment were subjected to SDS-PAGE and immunoblot analysis. **A to D.** Myo-DP did not induce inflammatory cytokine and chemokine expression, including *Il1b* (A), *Tnfa* (B), *Ccl2* (C), and *Il6* (D). In contrast, Myo-DP potently blocked the expression of these targets induced by LPS. **E.** Myo-DP did not induce NLRP3, INOS, and IL1B protein expression, while blocking LPS-induced protein targets. **F.** Myo-DP inhibited TNFA-triggered expression of *Ly6c*, *Il1b*, *Cxcl10*, and *Tnfa*. Two-way ANOVA.